Systemic loss of Sarm1 protects Schwann cells from chemotoxicity by delaying axon degeneration

Weili Tian*, Tim Czopka§ and Hernán López-Schier*

* Sensory Biology & Organogenesis, Helmholtz Zentrum Munich, Germany

§ Institute of Neuronal Cell Biology, Technical University of Munich, Germany

Correspondence to: hernan.lopez-schier@helmholtz-muenchen.de

Abbreviated title: Sarm1 and glioprotection

Keywords: Wallerian degeneration, Sarm1, Schwann cells, regeneration

ABSTRACT

Protecting the nervous system from chronic effects of physical and chemical stress is a pressing clinical challenge. The obligate pro-degenerative protein Sarm1 is essential for Wallerian axon degeneration. Thus, blocking Sarm1 function is emerging as a promising neuroprotective strategy with therapeutic relevance. Yet, the conditions that will most benefit from inhibiting Sarm1 remain undefined. Here we combine genome engineering, pharmacology and high-resolution intravital videmicroscopy in zebrafish to show that genetic elimination of Sarm1 increases Schwann-cell resistance to toxicity by diverse chemotherapeutic agents after axonal injury. Synthetic degradation of Sarm1-deficient axons reversed this effect, suggesting that glioprotection is a non-autonomous effect of delayed axon degeneration. Moreover, loss of Sarm1 does not affect macrophage recruitment to nerve-wound microenvironment, injury resolution, or neural-circuit repair. These findings anticipate that interventions aimed at inhibiting Sarm1 can counter heightened glial vulnerability to chemical stressors and may be an effective strategy to reduce chronic consequences of neurotrauma.

INTRODUCTION

The peripheral nerves that communicate skin, muscle and sensory organs with the brain must maintain functionality throughout life despite frequent stress and trauma (1-6). Loss of integrity of peripheral neurons and associated cells, including glia, is a common occurrence in severe neurological dysfunctions that include weakness, pain and loss of sensation (7). Glial loss leads to nerve demyelination, defasciculation and neuronal death. Nerve injury triggers axon fragmentation and degeneration. In turn, this induces the dedifferentiation of associated glial cells, which enhances glial role in nerve repair. However, dedifferentiation also makes glia vulnerable to degeneration after protracted denervation (8-12). Damaged axons undergo Wallerian degeneration (13), which is triggered by the evolutionary ancient pro-degenerative protein Sarm1 (Sterile Alpha and TIR Motif containing 1) (14-17). Sarm1 is a modular protein that contains two sterile-alpha motifs (SAM), one mitochondrial association (MT) and one TIR domain (14). Nerve injury activates Sarm1 by TIR dimerization, which is sufficient to induce the axon degeneration (18, 19). Mechanistically, Sarm1 activation results in the loss of nicotinamide adenine dinucleotide (NAD+) in damaged axons (20-22). The TIR domain acts as a NADase (23), explaining why over-expression of the NAD+ synthesizing enzyme NMNAT1 inhibits the degradation of severed axons by sustaining high levels of NAD+ downstream of Sarm1 (24). Moreover, the loss of Sarm1 blocks the degeneration of injured axons, and forced activation of Sarm1 induces axon destruction in the absence of injury. Therefore, Sarm1 is a hierarchical regulator of a signaling pathway that is necessary and sufficient for axonal degradation (22).

23 Upon peripheral-nerve injury, glial Schwann cells acquire a specialized function
24 that promotes the clearance of axon fragments ahead of axonal re-growth from the
25 proximal stump (25). Expeditious axonal regeneration is important because
26 sustained Schwann-cell denervation leads to protracted loss of glial terminal
27 phenotype and eventual death. In turn, glial loss impairs regenerating nerve
28 myelination and circuit repair, transforming acute neuropathies into irreversible
29 chronic neurological dysfunction. Therefore, inhibiting or delaying axon
30 destruction has been hypothesized as an effective strategy to counter heightened
31 Schwann-cell vulnerability to additional stressors that include metabolic imbalance
32 and drugs (26, 27). This idea has sparked intense efforts to identify specific
33 molecular inhibitors of axon degeneration for clinical applications (28, 29). As a
34 discrete hierarchical factor that is essential for axon degeneration, Sarm1 is an ideal
35 target for pharmacological interventions (18). However, the conditions that would
36 most benefit from inhibiting Sarm1 systemically are yet to be defined (30, 31). Here
37 we address the above issue using the powerful genetics of zebrafish, a small
38 vertebrate whose nervous system is anatomically simple but functionally similar to
39 that of mammals (32-34). Crucially, the zebrafish larva is ideal to study Schwann-
40 cell biology in the natural context of the behaving animal (35-42). By characterizing
41 loss-of-function mutations in Sarm1, we provide novel insights into the cellular basis
42 of axon-glia interactions, and provide data that encourage the quest to identify and
43 develop Sarm1 inhibitors for clinical applications.

44

45 **RESULTS**

46 **Identification and mutagenesis of Sarm1 in zebrafish**

47 The amino-acid sequence of Sarm1 is well conserved across species (15, 43). To
48 identify Sarm1 orthologs in zebrafish, we scanned publicly accessible genomic data
49 (***Danio rerio*** reference genome assembly version GRCz11) by a BLAST search
50 using the TIR domain, which is present in all known Sarm1 proteins (15, 44). This
51 exploration yielded a single candidate ***locus*** in chromosome 15. No other part of
52 the zebrafish genome appears to harbor Sarm1 paralogs. The genomic structure of
53 the putative zebrafish Sarm1 reminisces that of other species, containing 8 exons
54 that code for a protein of 713 amino acids, with the typical N-terminal auto-
55 inhibitory domain, two central SAM multimerization domains and a C-terminal
56 TIR degeneration domain (Figure 1A). Similar to ***D. melanogaster***, however, ***D.***
57 ***rerio*** Sarm1 lacks an obvious mitochondria-targeting sequence (MT). To test
58 whether the identified gene produces a protein with the expected functional role,
59 we used CRISPR/Cas9-mediated genome modification to generate loss-of-function
60 mutations in Sarm1. By targeting exon 1, we obtained germ-line transmission of
61 two alleles: ***sarm1***^{hzm13} and ***sarm1***^{hzm14} (Supplementary Figure 1A-B). The hzm13
62 allele introduces an 11-base deletion and T/C mutation, resulting in a frame shift
63 and premature stop codon. hzm14 is a 7-base deletion and AG/GA mutation that
64 also generates a frame shift and premature stop codon. Analysis of protein extracts
65 from wild-type embryos by Western-blot using an antibody to Sarm1 revealed a
66 single band of approximately 80kDa, which agrees with the expected size of the
67 full-length protein (Supplementary Figure 1C). This band was absent in protein

68 extracts from homozygous ***sarm1***^{hzm13} zebrafish embryos. Of note, because this
69 antibody recognizes an epitope in the C-terminus of Sarm1, it does not allow to
70 discriminate between the expression of a truncated protein lacking all the domains
71 with known function, and the complete absence of Sarm1 induced by nonsense-
72 mediated mRNA decay. Homozygous ***sarm1***^{hzm13} mutants display no overt
73 anatomical defects (Supplementary Figure 1D-E), are viable and develop into fertile
74 adults. Furthermore, a simple assay for sensorimotor function that consists of
75 eliciting the escape response after tactile stimuli showed that the displacement
76 distance and the average acceleration were no different between wild type and
77 Sarm1 mutants (Supplementary Figure 1F-G) (45).
78
79 **Functional conservation of Sarm1 in axon degeneration**
80 Although Sarm1 has already been extensively studied in neurons of ***Drosophila***
81 and mice, we deemed necessary to assess the effects of systemic loss of Sarm1 on
82 neuronal and non-neuronal cells in larval zebrafish. The reason is that no single
83 study has addressed Sarm1 function holistically, in a single organism, by intravital
84 high-resolution microscopy. To this end, we used several parameters of nervous-
85 system structure and function by combining ***sarm1***^{hzm13} with transgenes expressing
86 fluorescent markers in the sensory neurons of the mechanosensory lateral line, as
87 well as in their associated Schwann cells (46, 47). The lateral-line system is ideal for
88 such ***in vivo*** studies under normal and altered conditions (48-51). It combines the
89 organization of a typical vertebrate sensory system with the amenability for
90 controlled experimental interventions that include microsurgery, pharmacology and

91 optogenetics (41, 42, 52, 53). We found that loss of Sarm1 does not affect the
92 development and structure of the lateral-line sensory pathway (Supplementary
93 Figure 1H-N). For a more detailed analysis, we fluorescently marked mitochondria
94 in sensory neurons by expressing the mitochondria targeting sequence of the
95 Cytochrome-C oxidase subunit 8A fused to mCherry (54). We chose to study
96 mitochondria because they are dynamic organelles that distribute throughout the
97 neuron by active transport mediated by molecular motors that move along
98 microtubule tracks. In axons, microtubules are polarized such that their plus ends
99 are directed toward the axon terminals, in turn orienting the movement of distinct
100 molecular motors in the antero- and retro-grade directions (55). Intra-axonal
101 movement direction reflects mitochondrial fitness because stressed organelles are
102 biased in the retrograde direction (56, 57). Therefore, axonal mitochondria
103 represent an optimal proxy for neuronal polarization, intracellular dynamics and
104 overall health. We found a qualitatively similar number, density and distribution of
105 mitochondria in the peripheral axons of wild-type and Sarm1-mutant animals.
106 Kymographic analysis revealed a majority of static large mitochondrial groups, and
107 some smaller fragments moving substantial distances at constant velocity in the
108 anterograde and retrograde directions (Figure 1B-C). Importantly, quantifications
109 showed no significant differences in the number and spatial distribution of axonal
110 mitochondria (Figure 1D), or movement velocity and direction between wild-type
111 and Sarm1-mutant specimens (Figure 1E).
112

113 Next, we addressed functional conservation of Sarm1 in zebrafish using a
114 previously established bioassay of neurotrauma ***in vivo***, which employs laser-
115 mediated severing of individualized axons using single-neuron fluorescent-protein
116 expression and high-resolution microscopy (41,58). To precisely cut axons, we
117 focused an ultraviolet laser beam to a discrete region of the peripheral nerve. Upon
118 severing, the distal axon segment quickly degenerated in wild-type specimens,
119 whereas the proximal segment that stays associated with the neuronal perikaryon
120 remained viable (Figure 1F). Kinetic analysis shows that Sarm1-deficient severed
121 axons remained stable for over 5 days, whereas severed wild-type axons degraded
122 within 8 hours (Figure 1G). The degeneration-resistant phenotype of Sarm1
123 mutants was eliminated by the transgenic introduction of a fluorescent-tagged full-
124 length Sarm1 in mutant neurons (Figure 1H), demonstrating functional
125 conservation of zebrafish Sarm1.
126

127 **Loss of Sarm1 does not affect focal damage resolution**

128 Physical injury often results in inflammatory responses that recruit immune cells to
129 the wound. After nerve injury, injury-mediated production of reactive oxygen
130 species (ROS) as well as chemoattractants produced by Schwann cells recruits
131 inflammatory cells, including macrophages. Studies ***ex vivo*** using mammalian
132 cultured neurons showed that Sarm1 acts downstream of mitochondrial ROS
133 generation. Therefore, we decided to test ***in vivo*** if the loss of Sarm1 or the
134 absence of Schwann cells would affect macrophage recruitment to the site of injury.
135 To this end, we generated a transgenic line expressing membrane-targeted EGFP

136 under the control of the macrophage-specific promoter Mfap4. We combined this
137 line with Tg[SILL:mCherry] and mutations in Sarm1 or Erbb2. Loss of Erbb2 in
138 zebrafish impairs Schwann-cell migration along lateral-line axons and leads to
139 nerve unmyelination and defasciculation (53, 59). We injured nerves with a laser
140 and assessed macrophage behavior at high resolution. We found that the onset of
141 recruitment and number of macrophages at the wound did not differ between wild-
142 type specimens and Sarm1 or Erbb2 mutants (Figure 2A and Supplementary
143 Movies 1-3). Macrophages arrived from various locations and moved in a
144 qualitatively indistinguishable manner along the proximal and distal part of the
145 axons in wild-type and mutant specimens. Quantitative imaging showed that the
146 retention time of macrophages at the proximal side of the wound was unaltered in
147 Sarm1 or Erbb2 mutants, although on average retention was marginally lengthened
148 in the absence of Schwann cells (Figure 2B). In wild type, Sarm1 and Erbb2
149 mutants, macrophages engulfed debris locally at the injury site, and did not appear
150 to be involved in the degradation of the distal part of the severed axons
151 (Supplementary Movies 1-3). We found, however, a significant increase in the size
152 of the engulfed debris by macrophages in Erbb2-mutant animals (Figure 2C). These
153 results reveal that the loss of Sarm1 does not affect focal damage resolution by
154 macrophages. Also, importantly, they indicate that macrophages are recruited to
155 the wound independently of the Schwann cells. We did notice discrete and highly
156 mobile axon fragments that were not associated with EGFP(+) cells in wild-type
157 and Erbb2-mutant animals, but not in Sarm1-deficient fish.
158

159 **Synthetic degradation of severed Sarm1-deficient axons**

160 Calcium (Ca^{2+}) regulation in neurons is critical for homeostasis because sustained
161 elevation of cytosolic calcium leads to axonal and neuronal degeneration. Often,
162 this occurs because mitochondria release apoptosis-inducing factors and proteases
163 in a calcium-dependent manner (60). Studies of mammalian neurons ***in vitro*** and
164 of zebrafish have shown that neuronal damage triggers two waves of elevation of
165 axoplasmic calcium (Ca^{2+}) (21, 52). The first occurs nearly immediately after injury
166 and decays rapidly, whereas the second has slower onset and decay. Loss of Sarm1
167 prevents Ca^{2+} elevation in severed axons (21). We sought to further test the
168 functional conservation of Sarm1 in zebrafish ***in vivo*** by monitoring Ca^{2+}
169 dynamics in lateralis sensory axons at high-resolution before and after injury. We
170 measured Ca^{2+} dynamics ***in toto*** at high-resolution before and after axon injury
171 using the genetically-encoded ultrasensitive Ca^{2+} sensor GCaMP7a, to find that
172 intact wild-type and Sarm1-mutant axons show undetectable levels of axoplasmic
173 fluorescence above background (Figure 3A). Upon severing, fluorescent signal in
174 wild-type axons distal segments increased immediately and subsequently decayed
175 with a near constant slope, whereas fluorescence remained nearly undetectable in
176 Sarm1-deficient distal axon segments (Figure 3B). Next, we examined the Ca^{2+}
177 levels in mitochondria and the endoplasmic reticulum (ER) using genetically
178 encoded vital sensors, respectively Mito-RGECO and ER-GCaMP3 (Figure 3C-F).
179 We selected these organelles because Ca^{2+} release from the axonal ER activates the
180 mitochondrial permeability transition pore to trigger axonal degeneration (61, 62).
181 We found that both mitochondrial and reticular Ca^{2+} levels increased equally after

182 axon severing in severed wild-type and Sarm1-/- axons. These results reveal that
183 loss of Sarm1 attenuates calcium influx to the axoplasm, but not Ca^{2+} uptake in
184 mitochondria or the ER.
185
186 Because the second Ca^{2+} wave is responsible for the activation of the serine-
187 threonine protease Calpain, which in turn facilitates axonal fragmentation by
188 cleaving microtubules and neurofilaments (63), we decided to monitor Ca^{2+} levels in
189 lateralis sensory axons 2, 4, 8 and 12 hours-post-injury (hpi). In severed wild-type
190 axons, the second wave of axoplasmic Ca^{2+} starts 4 hpi in coincidence with axon
191 fragmentation, and remains elevated in axonal debris up until 8 hpi (Figure 4A).
192 Note that the temporal resolution of these images does not allow the resolution of
193 degeneration before axonal regeneration. By contrast, the second wave of
194 axoplasmic Ca^{2+} does not occur in Sarm1-mutant axons (Figure 4B). Thus, we
195 hypothesized that forcing a sustained elevation of axoplasmic Ca^{2+} will be sufficient
196 to trigger the degradation of severed Sarm1-deficient axons. To test this prediction,
197 we transgenically expressed the rat transient receptor potential cation channel
198 subfamily V member 1 (TRPV1) fused to tagRFP in lateralis afferent neurons of
199 Sarm1-mutant zebrafish. Expression of mCherry alone in neurons served as control.
200 TRPV1 is non-selective cation channel that exhibits a high divalent selectivity, and
201 whose activation produces an influx of Ca^{2+} into cells (64). Rat TRPV1 is activated
202 by temperatures above 43°C or by the vanilloid capsaicin. Importantly, this
203 TRPV1 is inactive at the temperature used to maintain zebrafish (28°C), and
204 zebrafish TRPV1 orthologs are insensitive to capsaicin (65). Therefore, rat TRPV1

205 expressed in zebrafish offers a tunable tool to elevate axoplasmic Ca^{2+} with
206 excellent temporal resolution. We severed TRPV1-expressing and mCherry-
207 expressing lateralis axons, and 2 hours later a vehicle solution or vehicle + capsaicin
208 were added in the water holding the fish (Supplementary Fgure 2A-B). Samples
209 were inspected 90 minutes later. Severed Sarm1-deficient axons not expressing
210 TRPV1 did not fragment in presence of capsaicin, or TRPV1-expressing axons
211 bathed in ethanol solution. As hypothesized, we found that Sarm1-deficient
212 TRPV1-expressing axon segments readily degraded in the presence of capsaicin
213 (Supplementary Figure 2C-F). These results demonstrate for the first time ***in vivo***
214 that elevation of axoplasmic Ca^{2+} downstream of Sarm1 is sufficient to trigger axon
215 degradation.
216
217 **Schwann cells are not essential to maintain Sarm1-/- axons**
218 The Schwann cells support, fasciculate and myelinate sensory axons in vertebrates
219 (66). We reasoned that delayed axon degeneration by loss of Sarm1 might impact
220 the interaction between axons and Schwann cells. To assess this interaction ***in vivo***,
221 we combined the ***sarm1***^{hzm13} allele with the triple transgenic line
222 ***Tg[gSAGFF202A ; UAS-GFP ; SILL:mCherry]*** to highlight the Schwann cells
223 with green fluorescence and the lateralis afferent neurons with red fluorescence (53,
224 67). Using high-resolution intravital microscopy, we ascertained that Schwann cells
225 develop normally and fasciculate sensory axons in Sarm1-deficient zebrafish (Figure
226 5A). Upon severing, wild-type axons were quickly cleared by the Schwann cells
227 through engulfment of axonal fragments and intracellular degradation of debris

228 (Figure 5B and Supplementary Movie 4). Thus, we asked if Schwann cells are
229 necessary for the maintenance of severed Sarm1-deficient axons by generating a
230 double mutant zebrafish line concurrently deficient for Erbb2 and Sarm1. In
231 Erbb2-deficient specimens, the distal portion of the severed axons fragmented and
232 were cleared (Figure 6A-B,D) but with a significant delay compared to wild-type
233 specimens (Figure 6A,D). By contrast, in Erbb2/Sarm1 double mutants, severed
234 axons did not fragment or degrade, identically to fish lacking only Sarm1 (Figure
235 6C,D). Thus, axon maintenance in Sarm1 mutants occurs independently of the
236 Schwann cells.
237
238 When an injury generates a gap in the glia, wound-adjacent Schwann cells actively
239 move and extend cellular projections resembling filopodia to quickly reconstitute a
240 continuous glial scaffold (53). Although continuous glia are not necessary for the re-
241 growth of the proximal axon stump, it prevents regenerating growth cones from
242 straying, in turn facilitating end-organ ***de novo*** innervation and circuit
243 reconstitution (39, 41). Thus, we decided to interrogate Schwann-cell behavior
244 immediately after axon severing and during axon regeneration combining
245 ***Tg[gSAGFF202A;UAS-GFP ; SILL:mCherry]*** double transgene with the Sarm1
246 mutation. As expected, we found that in wild-type animals, the Schwann cells
247 adjacent to the wound quickly extended filopodia to close the gap in the glial
248 scaffold ahead of axonal regeneration (Supplementary Movie 5). Re-growing fibers
249 then followed these sub-cellular glial bridges to reconstitute the nerve, suffering
250 mild defasciculation restricted to a small area within the injury (Figure 6E and

251 Supplementary Figure 3). In stark contrast, injury-adjacent Schwann cells did not
252 migrate or produce filopodia-like projections in Sarm1 mutants (Supplementary
253 Movie 6). Nonetheless, regenerating axons eventually negotiated the persistent
254 larger gap to grow along the distal glial scaffold. However, the reforming nerves
255 presented more pronounced local defasciculation (Figure 6F and Supplementary
256 Figure 4).
257
258 **Loss of Sarm1 does not alter Schwann-cell phenotype**
259 Denervated Schwann cells undergo partial dedifferentiation from myelinating to a
260 progenitor-like state as revealed by loss of expression of terminal-phenotype
261 markers, including myelin and myelin-associated proteins (25, 68, 69). The loss of
262 terminal phenotype promotes Schwann-cell proliferation and migration, which
263 enhances their regenerative function (70). We hypothesized that because Schwann-
264 cell denervation does not occur in Sarm1-mutants, distal Schwann cells may not
265 dedifferentiate. This would explain their lack of phagocytic and protrusive activities
266 after axon transection. Following this rationale, we immunostained samples with an
267 antibody to Claudin-k, which localizes to the junctions between mature Schwann
268 cells and is downregulated in denervated glia (41, 71). In wild-type specimens,
269 Claudin-k remained strongly expressed along the entire length of the lateralis
270 afferent nerve up to 6 hours after nerve injury (hpi), suggesting that distal Schwann
271 cells remain mature during distal-axon fragmentation (Figure 7A-B). Beginning at
272 10 hpi, however, distal Schwann cells had markedly less Claudin-k than proximal
273 cells. Finally, 24 hpi Claudin-k was conspicuously absent from distal Schwann cells

274 even after axons regeneration had commenced. By contrast, Claudin-k remained
275 strongly expressed after axon severing in Sarm1-mutant animals during the same
276 period, with no apparent difference between Schwann cells located at either side of
277 the wound (Figure 7A,C). Next, we assessed myelination using the 6D2 monoclonal
278 antibody, which recognizes a carbohydrate epitope in the piscine P0-like myelin
279 glycoproteins IP1 and IP2 (72, 73). As with Claudin-k, 6D2 labeling faded in
280 Schwann cells distal to the injury in wild-type specimens (Figure 8A). Yet, 6D2
281 labeling remained unchanged in Sarm1 mutants (Figure 8B). We obtained
282 congruent results when addressing myelination directly in living specimens by using
283 a transgenic line expressing membrane-targeted EGFP under the control of the
284 myelin binding protein (Mbp:EGFP-CAAX, green) (Figure 8C-D) (74).
285 Interestingly, forced degradation of Sarm1-deficient severed axons expressing the
286 rat TRPV1 channel after capsaicin treatment induced associated Schwann cells to
287 dedifferentiate (Supplementary Figure 2G). Together, these results indicate that
288 Sarm1-deficient sensory axons are maintained independently of Schwann-cell
289 support, and that the clearance the severed axons is not necessary for regenerating
290 axon growth, pathfinding, myelination and re-innervation of sensory organs. In
291 addition, they reveal that Schwann cells distal to the injury do not de-differentiate
292 in Sarm1-mutant specimens.
293
294 **Loss of Sarm1 protects Schwann cells from chemical toxins**
295 Many chemotherapeutic agents invariably cause peripheral neurotoxicity, leading
296 to permanent neuronal dysfunction (75-79). Under conditions of denervation,

297 Schwann cells become strongly susceptible to chemotoxicity (80). We wondered if
298 the protracted maintenance of severed axons in Sarm1 mutants may suppress glial
299 vulnerability. To test this idea, we treated wild-type and Sarm1-mutant zebrafish
300 with several chemical compounds that are under clinical trials or used as first-line
301 treatment for common cancers in humans. First, we used 10-Hydroxycamptothecin
302 (10-HCT), which is extremely toxic to denervated glia (82), and counted Schwann
303 cells using the fluorescence transgenic marker ***Tg[gSAGFF202A ; UAS:EGFP]***,
304 which is ideal for this experiment because the intensity of green fluorescence does
305 not vary in denervated Schwann cells and, therefore, is independent of the maturity
306 of these glia (41). We confirmed that 10-HCT does not affects in Schwann cells
307 associated to viable axon (Figure 9A-B). However, it significantly reduced the
308 number of Schwann cells in 10-HCT-treated wild-type animals after axon severing.
309 By contrast, the number of distal Schwann cells was only marginally affected in
310 Sarm1-mutant specimens (Figure 9B). Platinum-based, taxanes and some alkaloids
311 are effective chemotherapeutic agents used as standards-of-care for various human
312 malignancies, despite their severe neuropathic effects that include glial destruction
313 (81). To address their effect on Schwann cell, we treated wild-type or Sarm1 mutant
314 zebrafish with cisplatin, oxaliplatin, paclitaxel, docetaxel and vincristine. We found
315 that upon nerve transection, all these drugs invariably killed injury-distal Schwann
316 cells in wild-type specimens but not in Sarm1 mutants (Figure 9C). Importantly,
317 none of these drugs affected Schwann cells associated with intact axons, suggesting
318 that axons protect Schwann cells from chemical stress. To confirm this prediction,
319 we forced the degradation of severed axons in Sarm1-deficient zebrafish treated

320 with 10-HCT or vincristine. To this end, we repeated the used of capsaicin to
321 activate rat TRPV1 expressed in a sub-set of lateralis neurons in homozygous
322 mutant fish, in which Sarm1 is absent from every cell, including Schwann cells.
323 This experiment revealed that Schwann cells lacking Sarm1 again become
324 vulnerable to chemotoxicity once severed axons were synthetically eliminated
325 (Figure 9D), confirming that Sarm1-mediated glioprotection is non-autonomous
326 and depends upon the presence of non-degradable axons.
327

328 **DISCUSSION**

329 The sensory neurons that innervate skin, sensory receptors, joints and muscle
330 communicate peripheral information to the brain, enabling animals to perform the
331 essential activities of daily life. Using zebrafish and a battery of tests that include
332 subcellular structural characterization of sensory neurons and associated Schwann
333 cells, neuronal-function, and behavioral assays, we offer a comprehensive and
334 integrated analysis of neuronal and glial response to injury, as well as on the
335 consequences of blocking axon degeneration systemically. It has been well
336 established that the absence of Sarm1 in ***Drosophila*** and the mouse prevents the
337 degradation of damaged axons (15, 83). Although we were not predicting any
338 differences for Sarm1 in zebrafish, assaying functional conservation in our
339 experimental neuronal pathway is not dispensable because some neurotraumatic
340 conditions lead to neuronal loss in the absence of Sarm1. Loss of Sarm1 improves
341 functional recovery after traumatic brain injury in mice, and inhibits vincristine-
342 mediated neurotoxicity (84, 85). Sarm1-deficient mice are viable (19, 86). We found

343 that chronic and systemic loss of Sarm1 is compatible with zebrafish viability and
344 sensorineural function, and demonstrate that the long-term maintenance of non-
345 degradable axon fragments has no detrimental effect on the repair of a sensory
346 circuit. Furthermore, regenerating axons fasciculate and myelinate normally,
347 indicating that they do not compete with non-degradable axons segments for
348 exiting glia. Therefore, we conclude that the axonal destructive and nerve
349 reconstructive processes occur in parallel. In addition, these data suggest that a
350 competitive balance between axon degradation and regeneration does not appear
351 to have shaped the evolution of Sarm1 and, by extension, Wallerian degeneration.
352
353 Focusing on Schwann cells, we show that glial cells adjacent to nerve injury in
354 Sarm1 mutants behave dramatically different than those of wild-type specimens.
355 Specifically, Schwann cells in Sarm1 mutants do not migrate or extend projections
356 to bridge the gap in the glial scaffold, indicating that these cells do not directly sense
357 missing intercellular contacts or glial discontinuity. Instead, our findings suggest
358 alternative scenarios. One is that the degradation of axons releases signals that
359 induce Schwann cell to change behavior. In mice, for example, nerve damage
360 promotes mesenchymal behavior of Schwann cells surrounding the wound via
361 TGF-β signaling, which drives collective Schwann-cell migration across the wound
362 (87). Although we did not observe Schwann-cell migration, signals derived from
363 injured axons may promote wound-adjacent Schwann cells to extend projections to
364 bridge the gap in a similar manner. Interestingly, we observed that filopodia-like
365 structures emerged from Schwann cells at both sides of the injury in wild-type

366 animals, suggesting that repair-inducing signals are likely diffusible, affecting glial
367 cells independently of their association with axons. It remains to be determined if
368 the source of such signals is the damaged axons, the denervated Schwann cells, or
369 other cells in the wound microenvironment.
370
371 Upon nerve injury, activated macrophages rapidly accumulate around the wound
372 and contribute to Wallerian degeneration and to axonal regeneration. Specifically,
373 classical pro-inflammatory M1-type phagocytic macrophages remove axonal and
374 myelin debris, whereas anti-inflammatory M2-type macrophages modulate
375 Schwann-cell activity and promote axon regeneration (96). Immediately after nerve
376 injury, Schwann cells release chemokines that attract or retain macrophages at the
377 wound before axon fragmentation. Importantly, pharmacological activation of
378 macrophage recruitment to the wound microenvironment enhances axon
379 regeneration, whereas decrease of macrophage infiltration inhibits axon
380 regeneration. Reactive oxygen species (ROS) are conserved early wound signals
381 across species. Injury-mediated ROS production recruits inflammatory cells,
382 including macrophages. Primary sources of ROS after nerve damage are the
383 mitochondria and cellular NADPH oxidases. Studies in ***ex vivo*** cultured neurons
384 indicate that Sarm1 acts downstream of mitochondrial ROS generation. Also,
385 previous studies have characterized Wallerian axon degeneration and regeneration
386 in Erbb2 mutant specimens, but did not address effects on the wound
387 microenvironment and the behavior of macrophages (93-94). Accordingly, tested ***in***
388 ***vivo*** if the loss of Sarm1 as well as the absence of Schwann cells would affect

389 macrophage recruitment, to find that the onset of recruitment, the retention time
390 and number of macrophages at the wound did not differ between wild-type
391 specimens and Sarm1 or Erbb2 mutants. Also, as in wild-type specimens,
392 macrophages in Sarm1 and Erbb2 mutants engulfed debris locally, which were
393 larger within macrophages in Ebbr2 mutants. Thus, the loss of Sarm1 does not
394 affect focal damage resolution by macrophages, which are recruited and activated
395 independently of the Schwann cells. The above findings suggest that activated
396 phagocytic cells other than macrophages and Schwann cells, possibly neutrophils
397 (97), engulf and clear distal axon fragments after damage, and that this process does
398 not occur in Sarm1-deficient animals.
399
400 In conclusion, current mechanistic details about Sarm1 function derive from
401 independent observations extrapolated from a wide variety of experimental systems.
402 This has made it difficult to synthesize findings and reconcile some conflicting
403 observations. Here, we have exploited a powerful ***in vivo*** genetic system to
404 comprehensively study the consequence of systemic loss of Sarm1 from the sub-
405 cellular to the organismal level in a single vertebrate system. By generating
406 zebrafish carrying loss-of-function mutations in Sarm1, we confirmed and deepen
407 previous findings from ***Drosophila***, the mouse and cultured cells. Several novel
408 insights derive from the work presented here. First, that loss of Sarm1 is well
409 tolerated by the animal. Second, that neuronal-circuit repair is not contingent upon
410 rapid clearance of damaged axons. Third, that Schwann cells are not necessary for
411 maintenance of severed axons ***in vivo***. Fourth, that after the axotomy Schwann

412 cells distal to the cut site don't dedifferentiate in Sarm1-mutants ***in vivo***. Fifth, that
413 the protracted maintenance of transected axons dramatically improves Schwann-
414 cell tolerance to chemotoxicity after nerve injury after neurotrauma. This scenario
415 is likely to occur in the clinical setting because nerve trauma is an inescapable
416 consequence of surgical interventions, chronic metabolic dysfunction including
417 diabetes, and pharmacological treatments such as antibiotics and anæsthesia that
418 increase cellular stress (81). Therefore, these findings are of obvious
419 pathophysiological significance. Crucially, these data lend strong support to the
420 idea that direct interventions to systemically inhibit axon degradation are promising
421 strategies to reduce chronic consequences of neurotrauma. Because TIR domain
422 dimerization is necessary and sufficient to degrade NAD+, it renders Sarm1
423 amenable to inhibition by small molecules, as it has been demonstrated for the TIR
424 domain of TLR2 (95). Our findings encourage the development of Sarm1 inhibitors
425 for therapeutic applications (18, 29).
426
427
428
429
430
431
432
433
434
435
436

437 **METHODS**

438 **Zebrafish strains and husbandry**

439 Zebrafish (***Danio rerio***) were maintained in a centralized facility in accordance to
440 guidelines by the Ethical Committee of Animal Experimentation of the Helmholtz
441 Zentrum München, the German Animal Welfare act Tierschutzgesetz §11, Abs. 1,
442 Nr. 1, Haltungserlaubnis, to European Union animal welfare, and to protocols
443 number Gz.:55.2-1-54-2532-202-2014 and Gz.:55.2-2532.Vet_02-17-187 from the
444 "Regierung von Oberbayern", Germany. The transgenic lines Tg[UAS:EGFP],
445 Tg[HGn39D] and Tg[SILL:mCherry] (67), Tg[gSAGFF202A] (41),
446 Tg[UAS:GCaMP7a] (88), Tg[mbpa:tgRFP-CAAX]^{tum102Tg} (also known as
447 Tg[MBP:tgRFP]) (89) and Erbb2 mutants (41, 59) have been previously published.
448 The Tg[Sarm1-/-] was generated by CRISPR/Cas9 mediated mutagenesis.

449 **Sarm1 mutagenesis**

450 We used CRISPR/Cas9-mediated genome modification to generate mutations in
451 exon 1 of Sarm1. Cas9 mRNA and sgRNAs were co-injected into one-cell stage
452 embryos. Cas9 mRNA was generated ***in vitro*** from PmeI linearized CAS9 vector
453 (pMLM3613) using the Ambion™ mMESSAGE mMACHINE T7 Kit. The
454 mRNA was purified with the RNA easy kit (Qiagen). To generate the sgRNAs, the
455 target exon was sequenced and the sequence information was used to design
456 oligonucleotides for the sgRNA guide vector (pDR274) using the on-line tool
457 "ZiFiT Targeter software package" (http://zifit.partners.org***/)*** (90). The sgRNA
458 sequence for exon 1 of Sarm1 is 5'-GGGACTTGGAAGAGACCCGC-3'. The
459 annealed oligonucleotide was cloned into the BsaI-digested pDR274 vector using
460 T4 ligase (NEB M0202). Resulting clones were sequenced to verify correctness, and
461 then linearized with DraI. The purified linearized DNA fragment was employed to
462 generate the sgRNA using the T7 MEGAscript kit (Ambion™). By out-crossing
463 adult fish resulting from injection, we obtained germ-line transmission of two
464 independent alleles: ***sarm1***^{hzm13} and ***sarm1***^{hzm14}. For genotyping mutant carriers,
465 we used the primers: Forward: 5'-GATTTGCCGTTATCTCTCCA-3' and
466 Reverse: 5'-TCAAGCAGTTTGGCAGACTC-3'.

467 **DNA constructs**

468 The DNA constructs SILL:mCherry, SILL:Gal4 (67), UAS:Synapsin1-GFP (53)
469 and mbp:EGFP-CAAX have been previously described. The vectors pMLM3613
470 (42251) and pDR272 (42250) were purchased from Addgene. The plasmids
471 UAS:TRPV1-tagRFP, the coding sequence of rat TRPV1 containing the E600K
472 mutation fused to tagRFP was synthesized by Genecat and the expression construct
473 was generated using Tol2 kit. The constructs SILL:mito-mCherry, SILL:Sarm1-
474 v2a-mCherry, SILL:Kaede, SILL:mitoRGECO and SILL:erGCaMP3 were
475 generated using Tol2 kit. Mitochondria in lateralis neurons were marked by
476 expressing the mitochondria targeting sequence from the Cytochrome-C oxidase
477 subunit 8A fused to mCherry. The plasmids containing mito-RGECO and er-
478 GCaMP3 (92) were a gift of D.W. Raible (University of Washington).

479 **Antibodies and immunostaining**

480 Whole-mount immunostaining was performed as following. First, samples of
481 zebrafish embryos or larvae were fixed by immersion in ice-cold 4%
482 paraformaldehyde diluted into phosphate-buffered saline buffer containing 0.2%
483 Tween20 (PBST), and incubated overnight at 4°C. Then, the samples were washed
484 at room temperature (RT) with PBST three times, 10 minutes per wash, and
485 subsequently blocked in 10% bovine serum albumin (BSA), also at RT for 1 hour.
486 Next, the samples were incubated in primary antibodies at 4°C overnight. Next, the
487 samples were washed in PBST for 2 hours, changing to fresh buffer every 30
488 minutes. Finally, they were incubated with secondary antibodies at 4°C overnight.
489 Primary antibodies and concentrations: mouse anti-Acetylated tubulin, 1:1000
490 (Sigma T7251); rat anti-Claudin-k, 1:500 (gift from T. Becker, University of
491 Edinburgh, U.K.) (71); mouse 6D2, 1:5 (gift from Dr. G. Jeserich, University of
492 Osnabrück, Germany) (73). Secondary antibodies used were at the following
493 concentrations: donkey anti-Mouse Alexa Fluor® 555, 1:200, Abcam ab150106;
494 donkey anti-Rat IgG H&L (Alexa Fluor® 647) pre-adsorbed, 1:200, Abcam
495 ab150155). Samples were washed in PBST for 30 minutes and mounted in

496 Vectashield one day before microscopic examination. Imaging of fixed samples was
497 done with a laser-scanning confocal microscope (LSM 510, Carl Zeiss).

498 **Intravital microscopy**

499 For videomicroscopy, larvae were anesthetized with MS-222 (0.013% M/V) in
500 Danieau's and mounted in 0.8% low melting-point agarose on 35mm glass-bottom
501 Petri dishes. Samples were gently pressed against the glass using a hair-loop glued
502 to the tip of a glass pipette, as previously described. The agarose dome was
503 immersed in Danieau's with MS-222. Images of cells were acquired using a
504 spinning-disc microscope with a 40× air objective at 28.5°C (58). Z-stacks were set
505 to 0.8-1.2 μm intervals. Time intervals were 10 minute or 15 minute per stack. The
506 resulting raw data were processed, assembled and analyzed with ImageJ.

507 **Western blot assay**

508 Wild-type and mutant larvae were anesthetized and killed 5 days-post-fertilization.
509 Samples were homogenized in ice-cold RIPA buffer (with protease inhibitor
510 cocktail from Roche (Cat.04693159001). After homogenization, the samples were
511 incubated on ice for 30 minutes for further lysis. The resulting lysate was
512 centrifuged at 1200 rpm at 4°C, and the supernatant was taken for the BCA assay.
513 The supernatant was diluted in loading buffer and boiled at 99°C for 5 minutes.
514 Next, the samples were run in SDS-PAGE and transferred onto a PVDF
515 membrane. After blocking the membrane in 5% skimmed milk (diluted in PBST)
516 for 1 hour, the membrane was incubated with the primary antibody (rabbit anti-
517 Sarm1, 1:500, ANASPEC 55381; Mouse anti-β-Tubulin, 1:2000, Sigma T5168) at
518 4°C overnight. The next day, the membrane was washed and incubated with HRP-
519 labeled secondary antibody (Peroxidase-Affini Pure Goat Anti-Mouse IgG (H+L),
520 1:10000, Jackson Immuno Research 115035003; Peroxidase-Affini Pure Goat Anti-
521 Rabbit IgG (H+L), 1:10000, Jackson ImmunoResearch 115035144) for 1 hour.
522 Images were acquired by developing the membrane with ECL (Pierce™ ECL
523 Western Blotting Substrate, Thermo Fisher, 32109).
524
525

526 **Laser microsurgery**

527 To mark lateralis sensory neurons individually, DNA of the SILL:mCherry
528 construct was injected into eggs of Tg[HGn39D], Tg[HGn39D; Sarm1-/-],
529 Tg[SILL:mCherry; gSAGFF202A; UAS:EGFP] or Tg[SILL:mCherry ;
530 gSAGFF202A ; UAS:EGFP ; Sarm1-/-] zebrafish. Resulting larvae were selected
531 according to red-fluorescence in lateralis neurons. Selected samples were mounted
532 into agarose as described above, and their peripheral axons were targeted an
533 ultraviolet laser (350nm) using the iLasPulse system (Roper scientific AS, Evry,
534 France), as described previously. The laser beam was delivered using a 63x water-
535 immersion objective (50, 53, 58). The laser pulses were calibrated and applied to
536 the target area until a clear gap in the axons was visible. The samples were
537 observed again 1 hour post-injury (hpi) to confirm complete axon transection.

538 **Quantification of mitochondrial density and motility**

539 To analyze mitochondria in sensory axons, we generated kymographs of mito-
540 mCherry fluorescent spots using the Multi-Kymograph tool of the Fiji software
541 (http://fiji.sc). The movement of mitochondria was determined by the slope of the
542 lines drawn over time, and the direction of movement was determined by the
543 moving mitochondria crossing the time line (vertical) in the kymographs. The data
544 were analyzed with Python scripts and the Graphpad Prism software.

545 **Calcium imaging**

546 For calcium imaging in lateralis neurons, Tg[SILL:Gal4; UAS:GCaMP7a] double-
547 transgenic larvae were anesthetized and mounted in 0.8% low melting-point
548 agarose on a 35mm glass-bottom Petri dish. Imaging was acquired through a 63x
549 water-immersion objective with an exposure time of 400 milliseconds. Laser-
550 mediated axon transection was done after the 4th imaging of the time series. Next,
551 live videomicroscopy was done for 2 minutes at a frame rate of 400 milliseconds at
552 28.5°C. The raw data were analyzed with ImageJ. To quantify the calcium signal,
553 the images were processed to ImageJ. The region of interest (ROI) was selected and
554 measured the value with time point. GCaMP or RGECO intensity changes were
555 calculated as follows: $\Delta F/F0 = (F-F0)/F0$, where F0 is the value of the fluorescent

556 signal before axons were transected, and F is the value of the fluorescent signal with
557 time point after axon severing (92).

558 **Chemogenetics**

559 For chemogenetic experiments, we co-injected the SILL:Gal4 with UAS:mCherry
560 or UAS:ratTRPV1-tagRFP into the Tg[UAS:GCaMP7a] or Tg[HGn39D; Sarm1-
561 /-]. The positive larva with SILL:Gal4; UAS:ratTRPV1-tagRFP; UAS:GCaMP7a
562 expression was used to activate TRPV1 channels in zebrafish by incubation in 5μM
563 capsaicin (Sigma, M2028) and subsequent live imaging for 1hour of the mounted
564 and anesthetized embryo. Images were acquired through a 63x water-immersion
565 objective with an exposure time of 400 milliseconds. For experiments with the
566 Sarm1 mutant larvae, the HGn39D with SILL:mCherry or ratTRPV1-tagRFP
567 positive animals were laser axotomized. The larvae were treated with 10 μM
568 capsaicin or ethanol (1:1000, v/v) 2h after transection. 1.5h after capsaicin
569 treatment, images were taken by spinning disc microscopy.

570 **Behavioral assays**

571 For the touch-mediated escape response, 2dpf embryos were gently dechorionated
572 and kept in Danieau's solution at 28°C for at least 1 hour. Embryos were place into
573 a flat uncovered Petri dish containing Danieau's and were recorded with a high-
574 speed camera (NX4 series, Imaging solution, GmbH). Video recording was
575 launched and a randomly chosen embryo was touched with a blunt glass needle
576 until it evoked a reaction. Recordings were done under white-light illumination
577 over 150 seconds at a rate of 200 frames per second (fps). The swimming
578 trajectories were obtained with 3D Particle Tracker plugin, ImageJ software. The
579 further quantification and statistics were using Python.

580 **Statistics and Reproducibility**

581 The Student's t test (two tailed), ANOVA test, T-test (Tukey test) and Wilcoxon
582 rank sum test were applied using Python scripts. Error bars in all figures are
583 standard errors of the mean (SEM).

584

585

586

587 **REFERENCES**

588

589 1. Ameh V, and Crane S. Nerve injury following shoulder dislocation: the
590 emergency physician's perspective. ***Eur J Emerg Med.*** 2006;13(4):233-5.
591 2. Heneka MT, Carson MJ, El Khoury J, Landreth GE, et al. Neuroinflammation
592 in Alzheimer's disease. ***Lancet Neurol.*** 2015;14(4):388-405.
593 3. Missios S, Bekelis K, and Spinner RJ. Traumatic peripheral nerve injuries in
594 children: epidemiology and socioeconomics. ***J Neurosurg Pediatr.***
595 2014;14:688-94.
596 4. Rowe RK, Ellis GI, Harrison JL, Bachstetter AD, et al. Diffuse traumatic brain
597 injury induces prolonged immune dysregulation and potentiates hyperalgesia
598 following a peripheral immune challenge. ***Mol Pain.*** 2016;12.
599 5. Tzekov R, Phifer J, Myers A, Mouzon B, and Crawford F. Inflammatory
600 changes in optic nerve after closed-head repeated traumatic brain injury:
601 Preliminary study. ***Brain Inj.*** 2016;30(12):1428-35.
602 6. Ziogas NK, and Koliatsos VE. Primary Traumatic Axonopathy in Mice
603 Subjected to Impact Acceleration: A Reappraisal of Pathology and
604 Mechanisms with High-Resolution Anatomical Methods. ***J Neurosci.*** 2018;
605 38:4031-47.
606 7. Roselli F, and Caroni P. From intrinsic firing properties to selective neuronal
607 vulnerability in neurodegenerative diseases. ***Neuron.*** 2015;85(5):901-10.
608 8. Cattin AL, and Lloyd AC. The multicellular complexity of peripheral nerve
609 regeneration. ***Curr Opin Neurobiol.*** 2016;39:38-46.
610 9. Parrinello S, Napoli I, Ribeiro S, Wingfield Digby P, Fedorova M, Parkinson
611 DB, et al. EphB signaling directs peripheral nerve regeneration through Sox2-
612 dependent Schwann cell sorting. ***Cell.*** 2010;143(1):145-55.
613 10. Ziegenfuss JS, Doherty J, and Freeman MR. Distinct molecular pathways
614 mediate glial activation and engulfment of axonal debris after axotomy. ***Nat***
615 ***Neurosci.*** 2012;15(7):979-87.
616 11. Harrisingh MC, Pérez-Nadales E, Parkinson DB, Malcolm DS, Mudge AW,
617 and Lloyd AC. The Ras/Raf/ERK signalling pathway drives Schwann cell
618 dedifferentiation. ***EMBO J.*** 2004;23(15):3061-71.
619 12. Scherer SS. The biology and pathobiology of Schwann cells. ***Curr Opin***
620 ***Neurol.*** 1997;10(5):386-97.
621 13. Waller A. Experiments on the Section of the Glossopharyngeal and
622 Hypoglossal Nerves of the Frog, and Observations of the Alterations Produced
623 Thereby in the Structure of Their Primitive Fibres. ***Philosophical***
624 ***Transactions of the Royal Society of London.*** 1850;140:423-9
625 14. Gerdts J, Summers DW, Milbrandt J, and DiAntonio A. Axon Self-
626 Destruction: New Links among SARM1, MAPKs, and NAD+ Metabolism.
627 ***Neuron.*** 2016;89(3):449-60.
628 15. Osterloh JM, Yang J, Rooney TM, Fox AN, Adalbert R, Powell EH, et al.
629 dSarm/Sarm1 is required for activation of an injury-induced axon death
630 pathway. ***Science.*** 2012;337(6093):481-4.

631 16. Walker LJ, Summers DW, Sasaki Y, Brace EJ, Milbrandt J, and DiAntonio A.
632 MAPK signaling promotes axonal degeneration by speeding the turnover of the
633 axonal maintenance factor NMNAT2. ***Elife.*** 2017;6.
634 17. Yang J, Wu Z, Renier N, Simon DJ, et al. Pathological axonal death through a
635 MAPK cascade that triggers a local energy deficit. ***Cell.*** 2015;160:161-76.
636 18. Essuman K, Summers DW, Sasaki Y, Mao X, DiAntonio A, and Milbrandt J.
637 The SARM1 Toll/Interleukin-1 Receptor Domain Possesses Intrinsic NAD(+)
638 Cleavage Activity that Promotes Pathological Axonal Degeneration. ***Neuron.***
639 2017;93(6):1334-43 e5.
640 19. Gerdts J, Summers DW, Sasaki Y, DiAntonio A, and Milbrandt J. Sarm1-
641 mediated axon degeneration requires both SAM and TIR interactions. ***J***
642 ***Neurosci.*** 2013;33(33):13569-80.
643 20. Gerdts J, Brace EJ, Sasaki Y, DiAntonio A, and Milbrandt J. SARM1
644 activation triggers axon degeneration locally via NAD(+) destruction. ***Science.***
645 2015;348(6233):453-7.
646 21. Loreto A, Di Stefano M, Gering M, and Conforti L. Wallerian Degeneration Is
647 Executed by an NMN-SARM1-Dependent Late Ca(2+) Influx but Only
648 Modestly Influenced by Mitochondria. ***Cell Rep.*** 2015;13(11):2539-52.
649 22. Summers DW, Gibson DA, DiAntonio A, and Milbrandt J. SARM1-specific
650 motifs in the TIR domain enable NAD+ loss and regulate injury-induced
651 SARM1 activation. ***Proc Natl Acad Sci U S A.*** 2016;113(41):E6271-E80.
652 23. Essuman K, Summers DW, Sasaki Y, Mao X, Yim AKY, DiAntonio A, et al.
653 TIR Domain Proteins Are an Ancient Family of NAD(+)-Consuming Enzymes.
654 ***Curr Biol.*** 2018;28(3):421-30 e4.
655 24. Sasaki Y, Nakagawa T, Mao X, DiAntonio A, and Milbrandt J. NMNAT1
656 inhibits axon degeneration via blockade of SARM1-mediated NAD(+)
657 depletion. ***Elife.*** 2016;5.
658 25. Jessen KR, Mirsky R, and Lloyd AC. Schwann Cells: Development and Role
659 in Nerve Repair. ***Cold Spring Harb Perspect Biol.*** 2015;7(7):a020487.
660 26. Jortner BS. Mechanisms of toxic injury in the peripheral nervous system:
661 neuropathologic considerations. ***Toxicol Pathol.*** 2000;28(1):54-69.
662 27. Morell P, and Toews AD. Schwann cells as targets for neurotoxicants.
663 ***Neurotoxicology.*** 1996;17(3-4):685-95.
664 28. Koeppen AH. Wallerian degeneration: history and clinical significance. ***J***
665 ***Neurol Sci.*** 2004;220(1-2):115-7.
666 29. Simon DJ, and Watkins TA. Therapeutic opportunities and pitfalls in the
667 treatment of axon degeneration. ***Curr Opin Neurol.*** 2018;31(6):693-701.
668 30. Schuldiner O, and Yaron A. Mechanisms of developmental neurite pruning.
669 ***Cell Mol Life Sci.*** 2015;72(1):101-19.
670 31. Omura T, Omura K, Tedeschi A, Riva P, et al. Robust Axonal Regeneration
671 Occurs in the Injured CAST/Ei Mouse CNS. ***Neuron.*** 2015;86(5):1215-27.
672 32. D'Rozario M, Monk KR, and Petersen SC. Analysis of myelinated axon
673 formation in zebrafish. ***Methods Cell Biol.*** 2017;138:383-414.
674 33. Friedrich RW, Genoud C, and Wanner AA. Analyzing the structure and
675 function of neuronal circuits in zebrafish. ***Front Neural Circuits.*** 2013;7:71.

676 34. Friedrich RW, Jacobson GA, and Zhu P. Circuit neuroscience in zebrafish.
677 ***Curr Biol.*** 2010;20(8):R371-81.
678 35. Ackerman SD, Garcia C, Piao X, Gutmann DH, and Monk KR. The adhesion
679 GPCR Gpr56 regulates oligodendrocyte development via interactions with
680 Galpha12/13 and RhoA. ***Nat Commun.*** 2015;6:6122.
681 36. Bin JM, and Lyons DA. Imaging Myelination In Vivo Using Transparent
682 Animal Models. ***Brain Plast.*** 2016;2(1):3-29.
683 37. Fontenas L, and Kucenas S. Livin' On The Edge: glia shape nervous system
684 transition zones. ***Curr Opin Neurobiol.*** 2017;47:44-51.
685 38. Ohki Y, Wenninger-Weinzierl A, Hruscha A, Asakawa K, Haass C, et al.
686 Glycine-alanine dipeptide repeat protein contributes to toxicity in a zebrafish
687 model of C9orf72 associated neurodegeneration. ***Mol Neurodegener.***
688 2017;12(1):6.
689 39. Rosenberg AF, Isaacman-Beck J, Franzini-Armstrong C, and Granato M.
690 Schwann cells and deleted in colorectal carcinoma direct regenerating motor
691 axons towards their original path. ***J Neurosci.*** 2014;34(44):14668-81.
692 40. Wehner D, Tsarouchas TM, Michael A, Haase C, Weidinger G, Reimer MM,
693 et al. Wnt signaling controls pro-regenerative Collagen XII in functional spinal
694 cord regeneration in zebrafish. ***Nat Commun.*** 2017;8(1):126.
695 41. Xiao Y, Faucherre A, Pola-Morell L, Heddleston JM, Liu TL, Chew TL, et al.
696 High-resolution live imaging reveals axon-glia interactions during peripheral
697 nerve injury and repair in zebrafish. ***Dis Model Mech.*** 2015;8(6):553-64.
698 42. O'Donnell KC, Vargas ME, and Sagasti A. WldS and PGC-1alpha regulate
699 mitochondrial transport and oxidation state after axonal injury. ***J Neurosci.***
700 2013;33(37):14778-90.
701 43. Conforti L, Gilley J, and Coleman MP. Wallerian degeneration: an emerging
702 axon death pathway linking injury and disease. ***Nat Rev Neurosci.***
703 2014;15:394.
704 44. Howe K, Clark MD, Torroja CF, Torrance J, Berthelot C, Muffato M, et al.
705 The zebrafish reference genome sequence and its relationship to the human
706 genome. ***Nature.*** 2013;496(7446):498-503.
707 45. Sztal TE, Ruparelia AA, Williams C, and Bryson-Richardson RJ. Using
708 Touch-evoked Response and Locomotion Assays to Assess Muscle
709 Performance and Function in Zebrafish. ***J Vis Exp.*** 2016(116).
710 46. Ghysen A, and Dambly-Chaudière C. The lateral line microcosmos. ***Genes***
711 ***Dev.*** 2007;21(17):2118-30.
712 47. Pujol-Martí J, and López-Schier H. Developmental and architectural principles
713 of the lateral-line neural map. ***Front Neural Circuits.*** 2013;7:47.
714 48. Drerup CM, and Nechiporuk AV. In vivo analysis of axonal transport in
715 zebrafish. ***Methods Cell Biol.*** 2016;131:311-29.
716 49. Haehnel-Taguchi M, Akanyeti O, and Liao JC. Behavior, Electrophysiology,
717 and Robotics Experiments to Study Lateral Line Sensing in Fishes. ***Integr***
718 ***Comp Biol.*** 2018;58(5):874-83.
719 50. Pujol-Martí J, Faucherre A, Aziz-Bose R, Asgharsharghi A, Colombelli J,
720 Trapani JG, et al. Converging axons collectively initiate and maintain synaptic

721 selectivity in a constantly remodeling sensory organ. ***Curr. Biol.***
722 2014;24(24):2968-74.
723 51. Olt J, Ordoobadi AJ, Marcotti W, and Trapani JG. Physiological recordings
724 from the zebrafish lateral line. ***Methods Cell Biol.*** 2016;133:253-79.
725 52. Vargas ME, Yamagishi Y, Tessier-Lavigne M, and Sagasti A. Live Imaging of
726 Calcium Dynamics during Axon Degeneration Reveals Two Functionally
727 Distinct Phases of Calcium Influx. ***J Neurosci.*** 2015;35(45):15026-38.
728 53. Xiao Y, Tian W, and Lopez-Schier H. Optogenetic stimulation of neuronal
729 repair. ***Curr Biol.*** 2015;25(22):R1068-9.
730 54. Kim MJ, Kang KH, Kim CH, and Choi SY. Real-time imaging of
731 mitochondria in transgenic zebrafish expressing mitochondrially targeted GFP.
732 ***Biotechniques.*** 2008;45(3):331-4.
733 55. Mandal A, Pinter K, and Drerup CM. Analyzing Neuronal Mitochondria ***in***
734 ***vivo*** Using Fluorescent Reporters in Zebrafish. ***Front Cell Dev Biol.***
735 2018;6:144.
736 56. Lin MY, Cheng XT, Tammineni P, Xie Y, Zhou B, Cai Q, et al. Releasing
737 Syntaphilin Removes Stressed Mitochondria from Axons Independent of
738 Mitophagy under Pathophysiological Conditions. ***Neuron.*** 2017;94:595-610 e6.
739 57. Miller KE, and Sheetz MP. Axonal mitochondrial transport and potential are
740 correlated. ***J Cell Sci.*** 2004;117(Pt 13):2791-804.
741 58. Xiao Y, and López-Schier H. Studying Axonal Regeneration by Laser
742 Microsurgery and High-Resolution Videomicroscopy. ***Methods Mol Biol.***
743 2016;1451:271-80.
744 59. Lyons DA, Pogoda HM, Voas MG, Woods IG, Diamond B, Nix R, et al.
745 erbb3 and erbb2 are essential for schwann cell migration and myelination in
746 zebrafish. ***Curr Biol.*** 2005;15(6):513-24.
747 60. Ozaki T, Yamashita T, and Ishiguro S. Mitochondrial m-calpain plays a role in
748 the release of truncated apoptosis-inducing factor from the mitochondria.
749 ***Biochim Biophys Acta.*** 2009;1793(12):1848-59.
750 61. Court FA, and Coleman MP. Mitochondria as a central sensor for axonal
751 degenerative stimuli. ***Trends Neurosci.*** 2012;35(6):364-72.
752 62. Villegas R, Martinez NW, Lillo J, Pihan P, Hernandez D, Twiss JL, et al.
753 Calcium release from intra-axonal endoplasmic reticulum leads to axon
754 degeneration through mitochondrial dysfunction. ***J Neurosci.*** 2014;34:7179.
755 63. Park JY, Jang SY, Shin YK, Suh DJ, and Park HT. Calcium-dependent
756 proteasome activation is required for axonal neurofilament degradation.
757 ***Neural Regen Res.*** 2013;8(36):3401-9.
758 64. Caterina MJ, Schumacher MA, Tominaga M, Rosen TA, Levine JD, and
759 Julius D. The capsaicin receptor: a heat-activated ion channel in the pain
760 pathway. ***Nature.*** 1997;389(6653):816-24.
761 65. Gau P, Poon J, Ufret-Vincenty C, Snelson CD, Gordon SE, Raible DW, et al.
762 The zebrafish ortholog of TRPV1 is required for heat-induced locomotion. ***J***
763 ***Neurosci.*** 2013;33(12):5249-60.
764 66. Brosius LA, and Barres BA. Contrasting the glial response to axon injury in the
765 central and peripheral nervous systems. ***Dev. Cell.*** 2014;28(1):7-17.

766 67. Faucherre A, Pujol-Martí J, Kawakami K, and López-Schier H. Afferent
767 neurons of the zebrafish lateral line are strict selectors of hair-cell orientation.
768 ***PLoS One.*** 2009;4(2):e4477.
769 68. Sasaki Y, Hackett AR, Kim S, Strickland A, and Milbrandt J. Dysregulation of
770 NAD(+) Metabolism Induces a Schwann Cell Dedifferentiation Program. ***J***
771 ***Neurosci.*** 2018;38(29):6546-62.
772 69. Soto J, and Monje PV. Axon contact-driven Schwann cell dedifferentiation.
773 ***Glia.*** 2017;65(6):864-82.
774 70. Carr MJ, and Johnston AP. Schwann cells as drivers of tissue repair and
775 regeneration. ***Curr Opin Neurobiol.*** 2017;47:52-7.
776 71. Munzel EJ, Schaefer K, Obirei B, Kremmer E, Burton EA, Kuscha V, et al.
777 Claudin k is specifically expressed in cells that form myelin during development
778 of the nervous system and regeneration of the optic nerve in adult zebrafish.
779 ***Glia.*** 2012;60(2):253-70.
780 72. López-Schier H, and Hudspeth AJ. Supernumerary neuromasts in the
781 posterior lateral line of zebrafish lacking peripheral glia. ***Proc Natl Acad Sci***
782 ***U.S.A.*** 2005;102(5):1496-501.
783 73. Bastmeyer M, Jeserich G, and Stuermer CA. Similarities and differences
784 between fish oligodendrocytes and Schwann cells in vitro. ***Glia.*** 1994;11:300.
785 74. Czopka T, Ffrench-Constant C, and Lyons DA. Individual oligodendrocytes
786 have only a few hours in which to generate new myelin sheaths in vivo. ***Dev***
787 ***Cell.*** 2013;25(6):599-609.
788 75. Cavaletti G, Alberti P, and Marmiroli P. Chemotherapy-induced peripheral
789 neurotoxicity in the era of pharmacogenomics. ***Lancet Oncol.*** 2011;12:1151.
790 76. Kaiser J, Bledowski C, and Dietrich J. Neural correlates of chemotherapy-
791 related cognitive impairment. ***Cortex.*** 2014;54:33-50.
792 77. McLeary F, Davis A, Rudrawar S, Perkins A, and Anoopkumar-Dukie S.
793 Mechanisms underlying select chemotherapeutic-agent-induced
794 neuroinflammation and subsequent neurodegeneration. ***Eur J Pharmacol.***
795 2018;842:49-56.
796 78. Fukuda Y, Li Y, and Segal RA. A Mechanistic Understanding of Axon
797 Degeneration in Chemotherapy-Induced Peripheral Neuropathy. ***Front***
798 ***Neurosci.*** 2017;11:481.
799 79. Gornstein E, and Schwarz TL. The paradox of paclitaxel neurotoxicity:
800 Mechanisms and unanswered questions. ***Neuropharmacology.*** 2014;76:175.
801 80. Imai S, Koyanagi M, Azimi Z, Nakazato Y, Matsumoto M, Ogihara T, et al.
802 Taxanes and platinum derivatives impair Schwann cells via distinct
803 mechanisms. ***Sci Rep.*** 2017;7(1):5947.
804 81. Yang S, Abrahams MS, Hurn PD, Grafe MR, Kirsch JR. Local anesthetic
805 Schwann cell toxicity is time and concentration dependent. ***Reg Anesth Pain***
806 ***Med.*** 2011;36:444-51.
807 82. Bremer J, Skinner J, and Granato M. A small molecule screen identifies ***in***
808 ***vivo*** modulators of peripheral nerve regeneration in zebrafish. ***PLoS One.***
809 2017;12(6):e0178854.

810 83. Gilley J, Ribchester RR, and Coleman MP. Sarm1 Deletion, but Not Wld(S),
811 Confers Lifelong Rescue in a Mouse Model of Severe Axonopathy. ***Cell Rep.***
812 2017;21:10-6.
813 84. Henninger N, Bouley J, Sikoglu EM, An J, Moore CM, King JA, et al.
814 Attenuated traumatic axonal injury and improved functional outcome after
815 traumatic brain injury in mice lacking Sarm1. ***Brain.*** 2016;139(Pt 4):1094-105.
816 85. Geisler S, Doan RA, Strickland A, Huang X, Milbrandt J, and DiAntonio A.
817 Prevention of vincristine-induced peripheral neuropathy by genetic deletion of
818 SARM1 in mice. ***Brain.*** 2016;139(Pt 12):3092-108.
819 86. Turkiew E, Falconer D, Reed N, and Hoke A. Deletion of Sarm1 gene is
820 neuroprotective in two models of peripheral neuropathy. ***J Peripher Nerv***
821 ***Syst.*** 2017;22(3):162-71.
822 87. Clements MP, Byrne E, Camarillo Guerrero LF, Cattin AL, Zakka L, Ashraf A,
823 et al. The Wound Microenvironment Reprograms Schwann Cells to Invasive
824 Mesenchymal-like Cells to Drive Peripheral Nerve Regeneration. ***Neuron.***
825 2017;96(1):98-114 e7.
826 88. Muto A, Ohkura M, Abe G, Nakai J, and Kawakami K. Real-time
827 visualization of neuronal activity during perception. ***Curr Biol.*** 2013;23:307.
828 89. Auer F, Vagionitis S, and Czopka T. Evidence for Myelin Sheath Remodeling
829 in the CNS Revealed by ***In Vivo*** Imaging. ***Curr Biol.*** 2018;28(4):549-59 e3.
830 90. Wright DA, Thibodeau-Beganny S, Sander JD, Winfrey RJ, Hirsh AS,
831 Eichtinger M, et al. Standardized reagents and protocols for engineering zinc
832 finger nucleases by modular assembly. ***Nat Protoc.*** 2006;1(3):1637-52.
833 91. Czopka T, and Lyons DA. Individual oligodendrocytes have only a few hours
834 in which to generate new myelin sheaths ***in vivo***. ***Dev. Cell.*** 2013;25(6):599.
835 92. Esterberg R, Linbo T, Pickett SB, Wu P, Ou HC, Rubel EW, et al.
836 Mitochondrial calcium uptake underlies ROS generation during
837 aminoglycoside-induced hair cell death. ***J Clin Invest.*** 2016;126(9):3556-66.
838 93. Atanasoski, S., Scherer, S. S., Sirkowski, E., Leone, D., Garratt, A. N.,
839 Birchmeier, C., & Suter, U. ErbB2 signaling in Schwann cells is mostly
840 dispensable for maintenance of myelinated peripheral nerves and proliferation
841 of adult Schwann cells after injury. ***J. Neurosci.*** 2006; 26: 2124-31.
842 94. Han, S. B., Kim, H., Lee, H., Grove, M., Smith, G. M., & Son, Y. J. Postinjury
843 induction of activated ErbB2 selectively hyperactivates denervated Schwann
844 cells and promotes robust dorsal root axon regeneration. ***J. Neurosci.*** 2017;
845 37: 10955–10970.
846 95. Mistry P, Laird MH, Schwarz RS, Greene S, Dyson T, Snyder GA, et al.
847 Inhibition of TLR2 signaling by small molecule inhibitors targeting a pocket
848 within the TLR2 TIR domain. ***Proc.Natl.Acad.Sci.U.S.A.*** 2015; 112:5455-60.
849 96. Kigerl KA, Gensel JC, Ankeny DP, Alexander JK, Donnelly DJ, Popovich PG.
850 Identification of two distinct macrophage subsets with divergent effects causing
851 either neurotoxicity or regeneration in the injured mouse spinal cord. ***J.***
852 ***Neurosci***. 2009; 29(43):13435-44.

97. Lindborg JA, Mack M, Zigmond RE. Neutrophils Are Critical for Myelin Removal in a Peripheral Nerve Injury Model of Wallerian Degeneration. ***J. Neurosci***. 2017; 37(43):10258-10277

FIGURE LEGENDS

Figure 1. a) Structure Sarm1 indicating alignment of the Sarm1 functional domains from different species (not at scale). **b)** Confocal image of axonal mitochondria marked with mito-mCherry in wild-type and Sarm1-/-. Red arrows point to prominent mitochondrial groups in axons. **c)** Upper panels, kymographs from videomicroscopic recording of axonal mitochondria in wild type (H) (left panel) and Sarm1-/- (I) (right panel). Lower panels show color-coded traces of moving mitochondria in anterograde (green) and retrograde (red) directions, taken from the kymographs shown in the upper panels. **d)** Density of mitochondria in 5dpf wild type and Sarm1-/-, Error bar = SEM; n.s. = not significant, p value from Student's t test, n=25 (WT), n=19 (Sarm1-/-). **e)** Mobility of the mitochondria in 5dpf wild type and Sarm1-/-. Circles show the anterograde and triangles the retrograde movement of the mitochondria. p value from one-way ANOVA, wild type n=26, Sarm1-/- n=26. **f)** Time-lapse images of axonal degeneration of GFP-labeled lateralis sensory neuron in wild-type (left) and Sarm1-/- larvae (right). hpi = hour post injury, scale bar=50μm, white asterisk indicates the regrowing axons from the proximal stump. **g)** Quantification of the time from axon transection to fragmentation in wild type (n=13) and Sarm1-/- (n=13). **h)** Shows a recue experiment in which the expression of a functional Sarm1 in sensory neurons of Sarm1-mutant fish (right hand side panels) suffices to degrade severed axons, similarly to wild-type fish (left hand side panels). Middle panels show non-degradable Sarm-1 deficient severed axons.

884 **Figure 2. a)** Quantification of the number of macrophages recruited to the injury
885 site and adjacent axon segments. **b)** Quantification of the time macrophages
886 interact with axon segments. **c)** Quantification of the size of debris within
887 macrophages. One-way ANOVA was conducted firstly, then P values for T-test in
888 between two individual group.
889
890 **Figure 3. a)** Confocal image of a single lateralis sensory axon expressing the
891 green-fluorescent calcium sensor GCaMP7a in wild type (left column) and Sarm1-
892 /- fish (right column). Rows show that same samples before laser-mediated
893 transection (top), immediately after transection (middle) and 60 seconds after
894 transection (bottom). In A, C and E, white arrowheads indicate the position of the
895 axon, specifically when signal-to-background is low. Scale bar 20μm. **b)** Shows
896 quantification of the first wave of axoplasmic calcium. Data are shown as mean ±
897 SEM; p from one-way ANOVA, wild type n = 16, Sarm1-/- 16. **c)** Shows a
898 confocal image of lateralis sensory axons expressing the red-fluorescent calcium
899 sensor RGECO in wild type (left column) and Sarm1-/- fish (right column). Rows
900 show that same samples before laser-mediated transection (top), immediately after
901 transection (middle), and 60 seconds after transection (bottom). **d)** Quantification
902 mitochondrial calcium influx shows the strong and nearly identical elevation and
903 decay in wild type and Sarm1-/- immediately after the cuts. Data are shown as
904 mean ± SEM; p from one-way ANOVA, wild type n = 16, Sarm1-/- 16. **e)** Shows
905 a confocal image of lateralis sensory axons expressing the green-fluorescent calcium
906 sensor CCaMP3 targeted to the endoplasmic reticulum (ER) in wild type (left
907 column) and Sarm1-/- fish (right column). Rows show that same samples before
908 laser-mediated transection (top), immediately after transection (middle), and 60
909 seconds after transection (bottom). **f)** Quantification ER calcium influx shows
910 strong and statistically equal elevation and decay in wild type and Sarm1-/- after
911 the cuts. Data are shown as mean ± SEM; p from one-way ANOVA, wild type n =
912 16, Sarm1-/- 16.
913

914 **Figure 4. a)** Confocal image of a lateralis sensory axons expressing the mCherry
915 (red) and green-fluorescent calcium sensor GCaMP7a (green) in wild type fish.
916 Rows show same axons 2, 4, 8 and 12 hours after transection (hours-post-injury =
917 hpi). **b)** Confocal image of lateralis sensory axons expressing the mCherry (red) and
918 green-fluorescent calcium sensor GCaMP7a (green) in Sarm1-/- fish. Scale bar
919 20μm.
920
921 **Figure 5. a)** Confocal images of a double transgenic 5dpf larva showing Schwann
922 cells marked by expression of GFP (green) under the control of the
923 Tg[gSAGFF202A] Gal4 driver, and lateralis afferent neurons marked by expression
924 of mCherry under the control of the SILL enhancer (red). Wild type (top), Sarm1
925 mutants (bottom). Scale bar 20μm. **b)** Images show the indicated time points after
926 axon transection (hours post injury = hpi) from a videomicroscopic recording of
927 Schwann cells (green) and their interaction with axons (red) in wild-type and
928 Sarm1-/-. White arrowheads indicate Schwann cells engulfing axonal debris in the
929 wild type. A white arrow indicates degradation-resistant axon segment in Sarm1-/-.
930 Please, note that the proximal axon stump in Sarm1-/- is not visible in these images
931 because it is outside the focal plane.
932
933 **Figure 6. a-c)** Images of mCherry-expressing (red) transected axons in wild type
934 (A), Erbb2-/- mutants (B), and Sarm1-/- ; ErBb2-/- double mutants (C). Scale bar
935 100μm. **d)** Quantification of transected axon fragmentation in Erbb2-/- and
936 Sarm1-/-; ErBb2-/-. Error bar = SEM, p value from One-way ANOVA test, n =
937 15 (each group). **e)** Image of a from Supplemental Movie 1, showing the discrete
938 local defasciculation of regenerated the sensory fiber (red) and the bridging of the
939 glial gap by Schwann cells (green) in a wild-type specimen. **f)** Equivalent
940 experiment, taken from Supplemental Movie 2, showing a more pronounced local
941 defasciculation of the regenerated the sensory fiber (red) in a Sarm1-mutant
942 specimen. Note that and the bridging of the glial gap does not occur.
943

944 **Figure 7. a-c)** Schematic model of the confocal imaging locations on severed
945 axons (A). Confocal images of wild type (B) and Sarm1-/- (C) specimens in 6hpi,
946 10hpi and 24hpi. hpi = hour post injury. The specimens were the
947 Tg[gSAGFF202A;UAS:EGFP; SILL:mCherry] lines and were stained with
948 Claudin-k (magenta) antibody. Scale bar 50μm.
949
950 **Figure 8. a-b)** Confocal images of wild type (A) and Sarm1-/- (B) specimens
951 expressing EGFP in sensory neurons of the lateral line (green) and stained with the
952 monoclonal antibody 6D2. Stainings were performed at indicated time points after
953 axons severing (hpi). The arrows point to the cutting sites. Scale bar is 50μm. **c)**
954 Live imaging of the ***Tg[Mbp-EGFP; SILL:mCherry]*** after severing. The arrows
955 indicated the fragmented axons and the arrowheads the fragmented myelin. Scale
956 bar 20μm. **d)** Live imaging of the Sarm1-/- in ***Tg[Mbp-EGFP; SILL:mCherry]***
957 after severing. Arrows indicate regrowing axons, and arrowheads indicate the
958 juxtaposition between the regrowing axons. Scale bar 20μm.
959
960 **Figure 9. a)** Confocal images showing Schwann cells (green) and lateralis sensory
961 axons (red) in a control specimen (in which axons were not transected), in a
962 specimen 48 hours after axon transection, and in specimens treated with 10-HCT
963 (10-Hydroxycamptothecin). Left column is wild type and right column shows
964 Sarm1-/-. In all cases, the concentration of 10-HCT in water was 40μm. Scale bar
965 100μm. **b)** Quantification of the Schwann cells from A). Data are shown as mean ±
966 SEM. ** means $p < 0.01$, two-way ANOVA, n = 8 (each group), followed by T-test
967 for two individual group. **c)** Quantification of Schwann cells of WT, WT severed,
968 Sarm1-/- and Sarm1-/- severed with the treatment of the indicated chemical
969 compounds for 48 hours. Concentrations: Paclitaxel 40μm, Docetaxel 0.1μm,
970 Oxaliplatin 500μm, Cisplatin 50μm, Vincristine 50μm. Data are shown as mean ±
971 SEM. * means $p < 0.05$; ** means $p < 0.01$, three-way ANOVA, n = 8 (each
972 group), followed by T-test for two individual group. **d)** Quantification of Schwann
973 cells after axon severing, in specimens treated with 10-HCT or Vincristine. Left bar

974 group is wild type. Right bar group is Sarm1-/-, and Sarm1-/- with synthetically
975 eliminated axon segments. Two-way ANOVA, followed by T-test for two
976 individual groups.

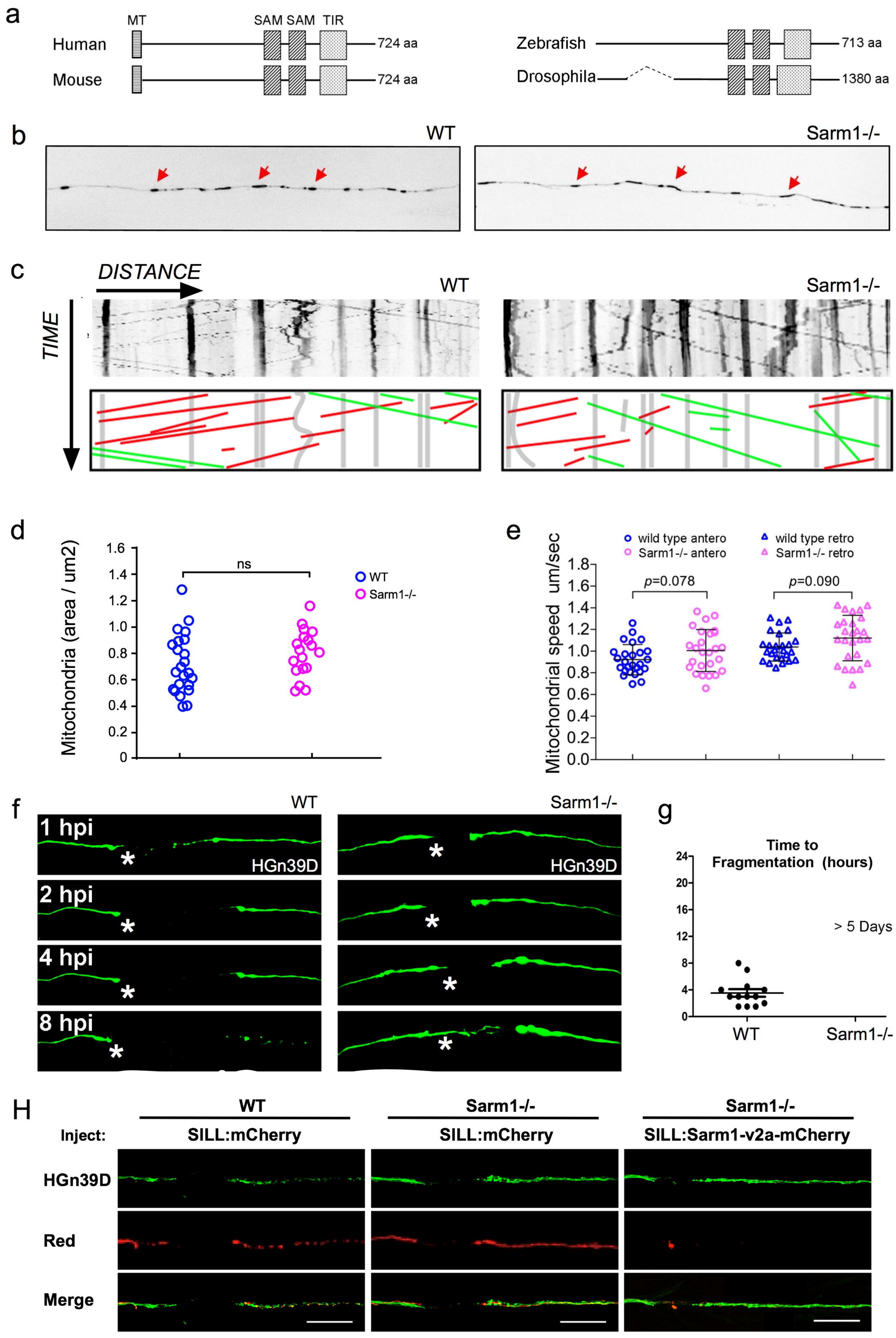
a
MT
SAM SAM TIR
Human
Mouse
724 aa
724 aa
Zebrafish
Drosophila
713 aa
1380 aa
b
WT
Sarm1-/-
c
DISTANCE
TIME
WT
Sarm1-/-
d
Mitochondria (area / um2)
ns
WT
Sarm1-/-
e
Mitochondrial speed um/sec
wild type antero
Sarm1-/- antero
wild type retro
Sarm1-/- retro
p=0.078
p=0.090
f
WT
Sarm1-/-
1 hpi
2 hpi
4 hpi
8 hpi
HGn39D
g
Time to Fragmentation (hours)
> 5 Days
WT
Sarm1-/-
H
WT
Sarm1-/-
Sarm1-/-
Inject:
SILL:mCherry
SILL:mCherry
SILL:Sarm1-v2a-mCherry
HGn39D
Red
Merge

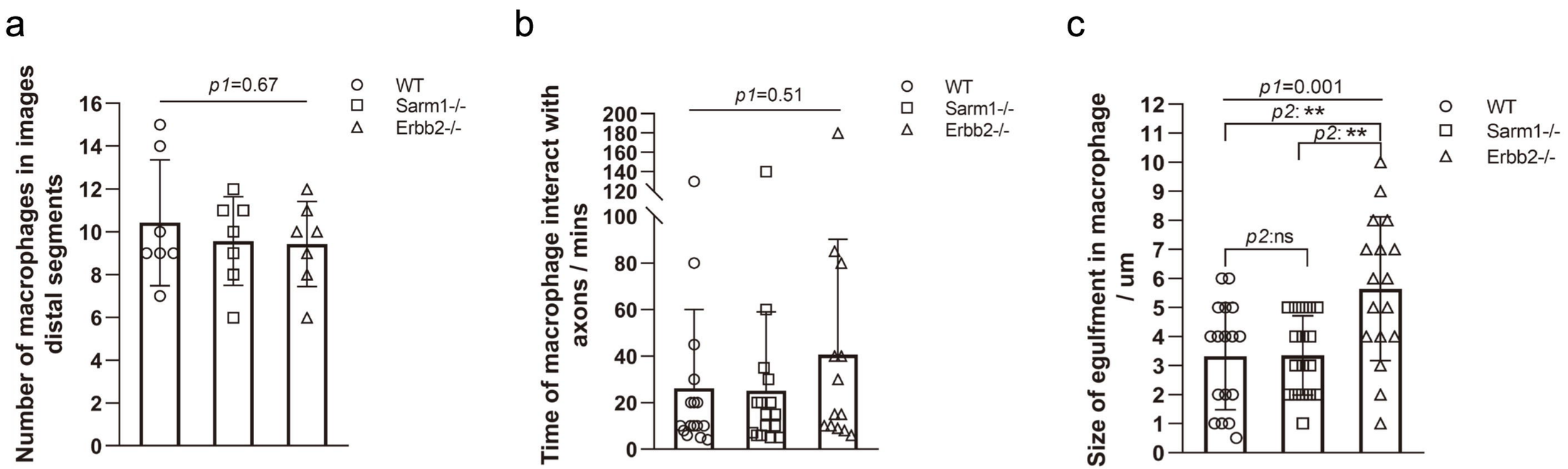
a
Number of macrophages in images distal segments
p1=0.67
WT
Sarm1-/-
Erbb2-/-
b
Time of macrophage interact with axons / mins
p1=0.51
WT
Sarm1-/-
Erbb2-/-
c
Size of egulfment in macrophage / um
p1=0.001
p2: **
p2: **
p2:ns
WT
Sarm1-/-
Erbb2-/-

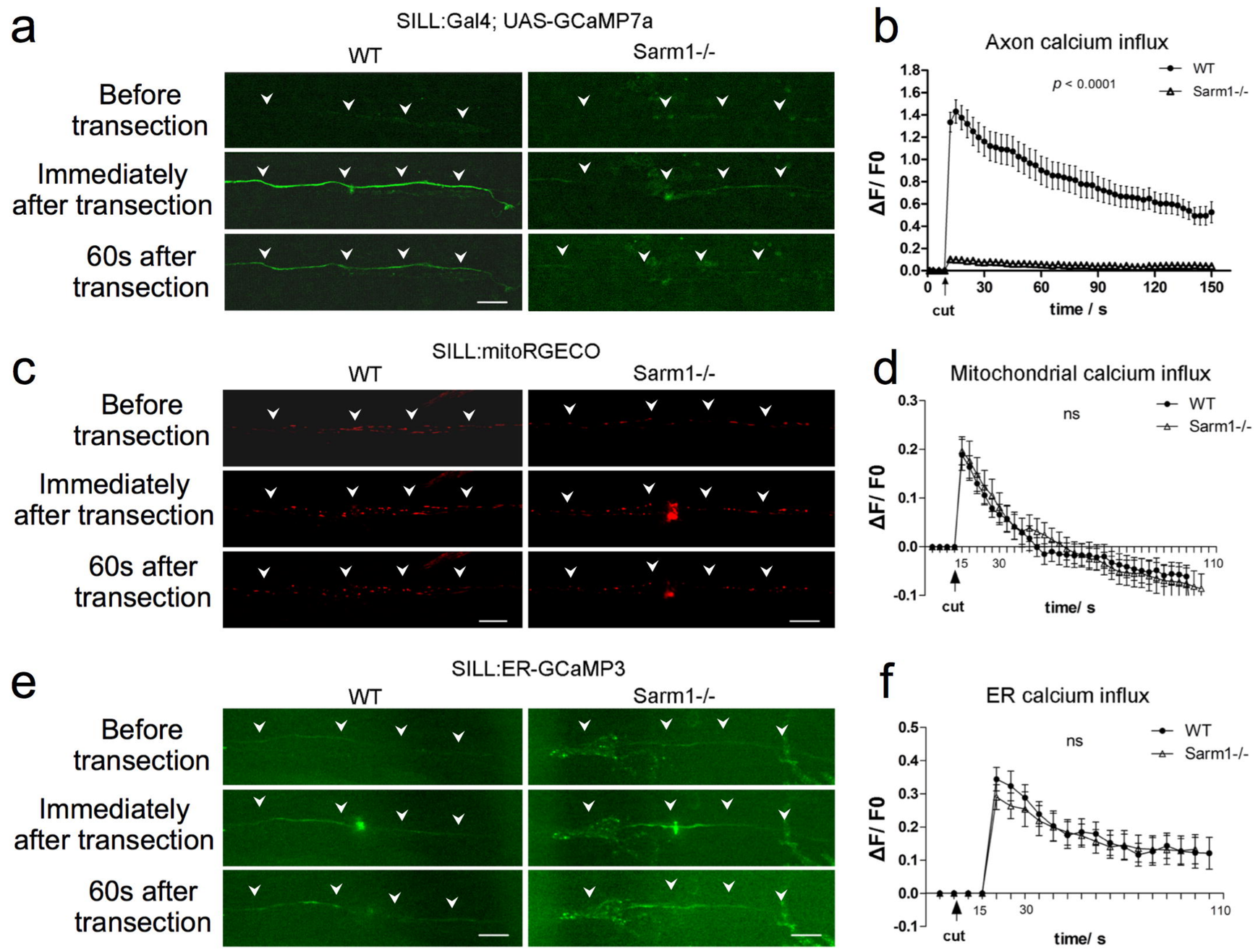
a
SILL:Gal4; UAS-GCaMP7a
WT
Sarm1-/-
Before transection
Immediately after transection
60s after transection
b
Axon calcium influx
p < 0.0001
WT
Sarm1-/-
ΔF/ F0
cut
time / s
c
SILL:mitoRGECO
WT
Sarm1-/-
Before transection
Immediately after transection
60s after transection
d
Mitochondrial calcium influx
ns
WT
Sarm1-/-
ΔF/ F0
cut
time/ s
e
SILL:ER-GCaMP3
WT
Sarm1-/-
Before transection
Immediately after transection
60s after transection
f
ER calcium influx
ns
WT
Sarm1-/-
ΔF/ F0
cut
time/ s

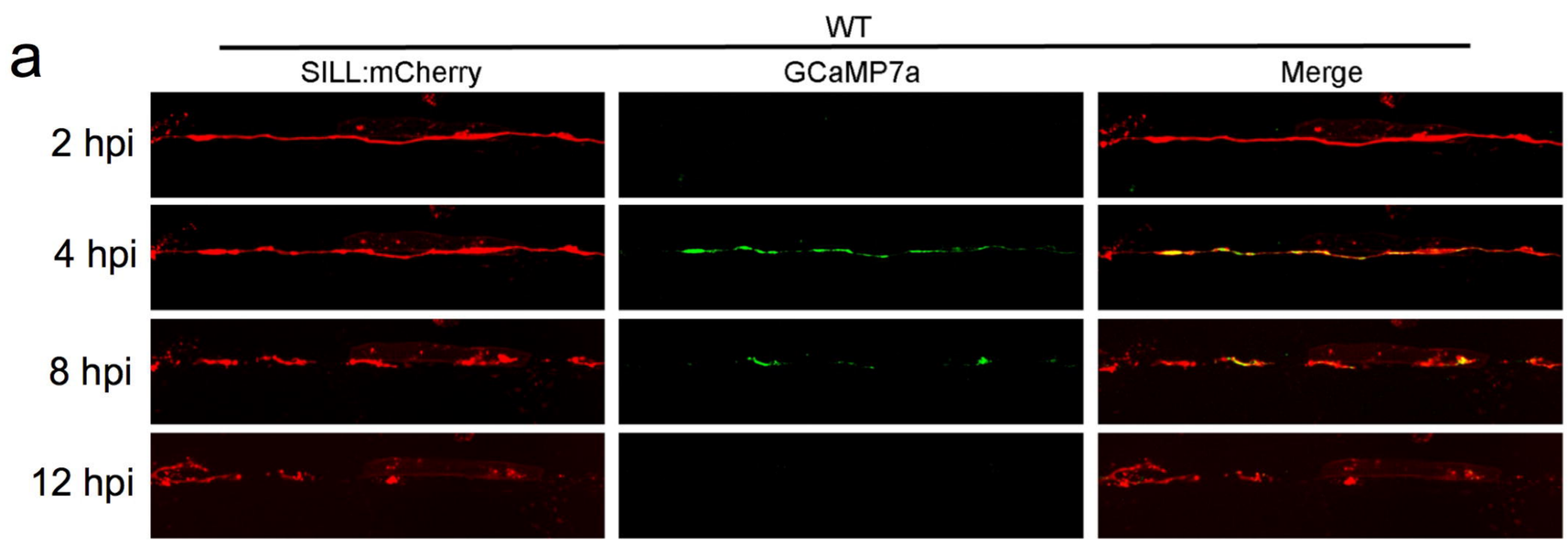
a
WT
SILL:mCherry
GCaMP7a
Merge
2 hpi
4 hpi
8 hpi
12 hpi

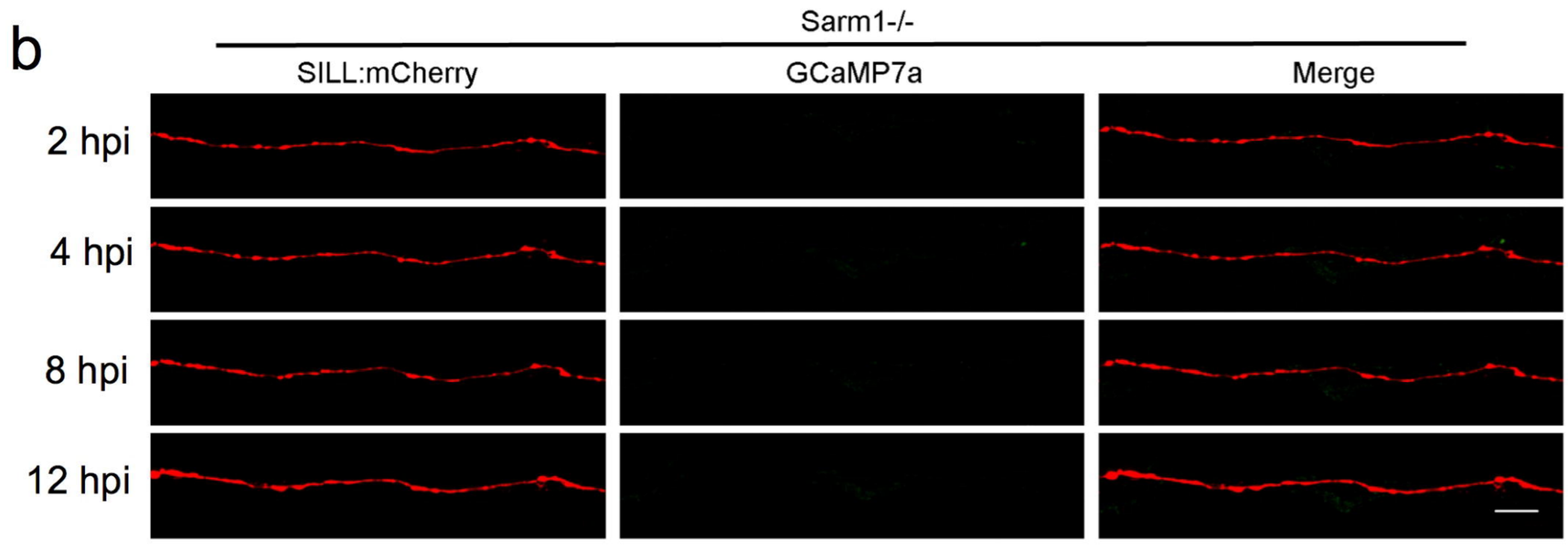
b
Sarm1-/-
SILL:mCherry
GCaMP7a
Merge
2 hpi
4 hpi
8 hpi
12 hpi

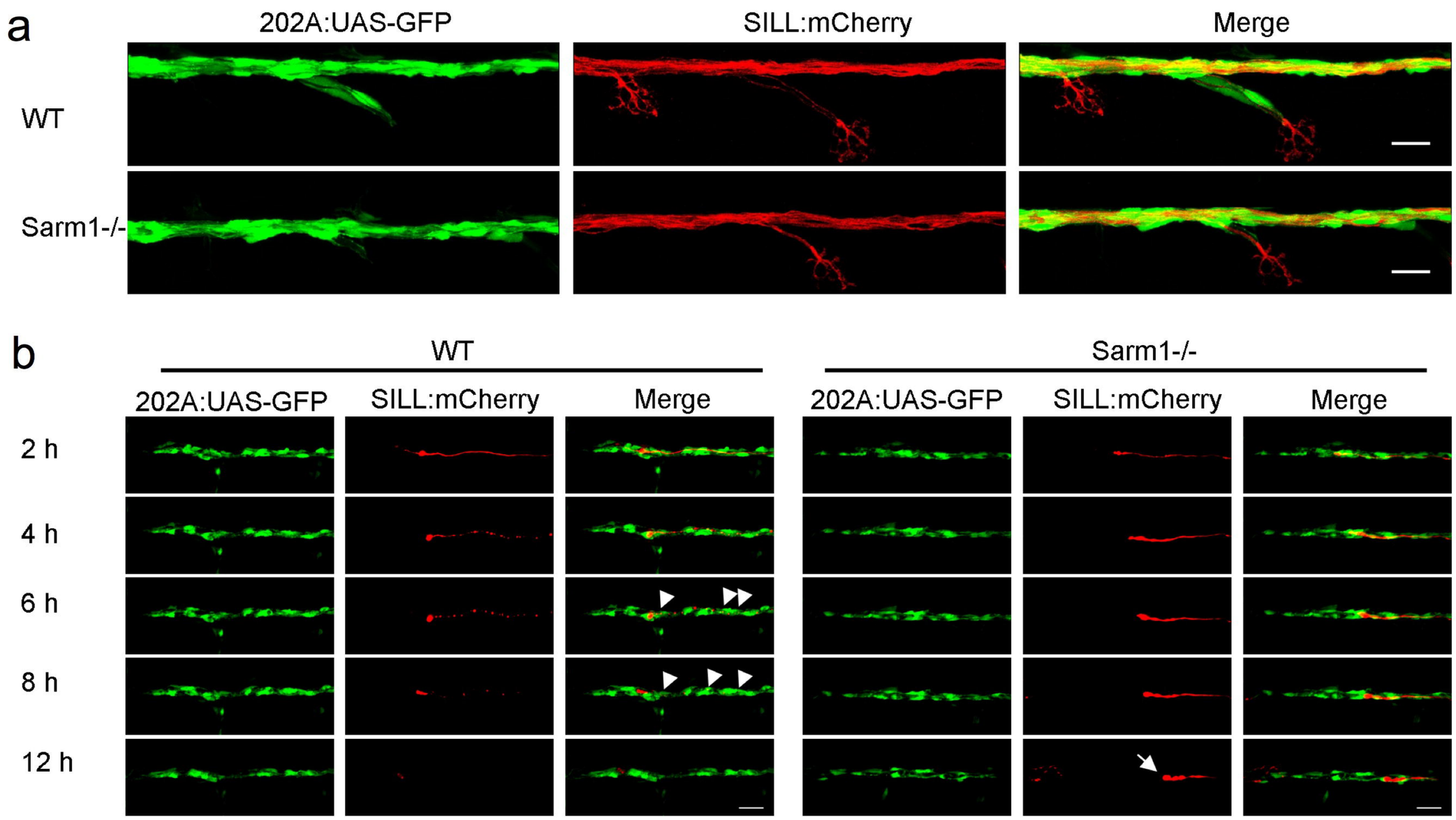
a
202A:UAS-GFP
SILL:mCherry
Merge
WT
Sarm1-/-
b
WT
Sarm1-/-
202A:UAS-GFP
SILL:mCherry
Merge
202A:UAS-GFP
SILL:mCherry
Merge
2 h
4 h
6 h
8 h
12 h

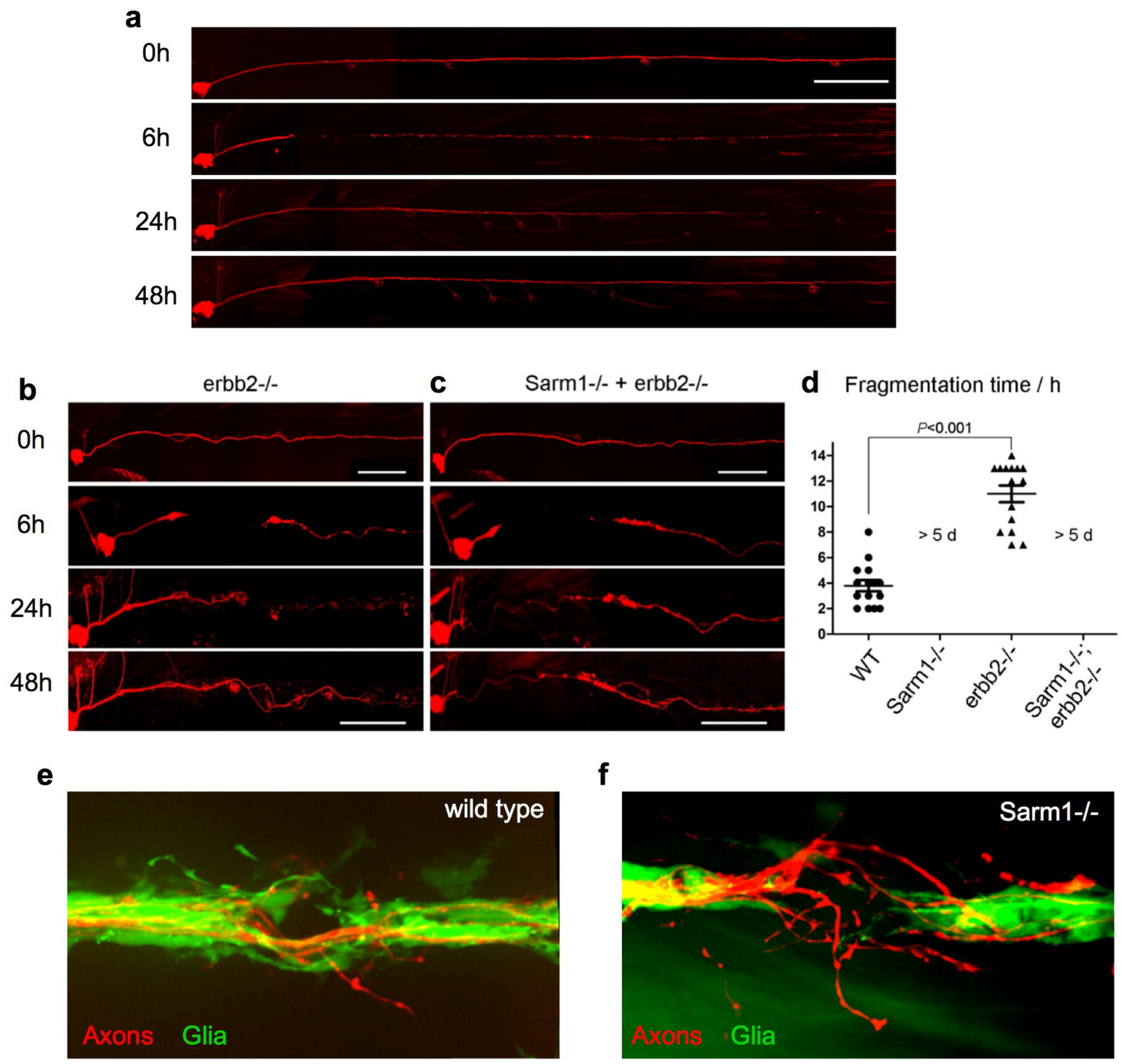
a
0h
6h
24h
48h
b
erbb2-/-
c
Sarm1-/- + erbb2-/-
0h
6h
24h
48h
d
Fragmentation time / h
P<0.001
> 5 d
> 5 d
WT
Sarm1-/-
erbb2-/-
Sarm1-/-; erbb2-/-
e
wild type
Axons
Glia
f
Sarm1-/-
Axons
Glia

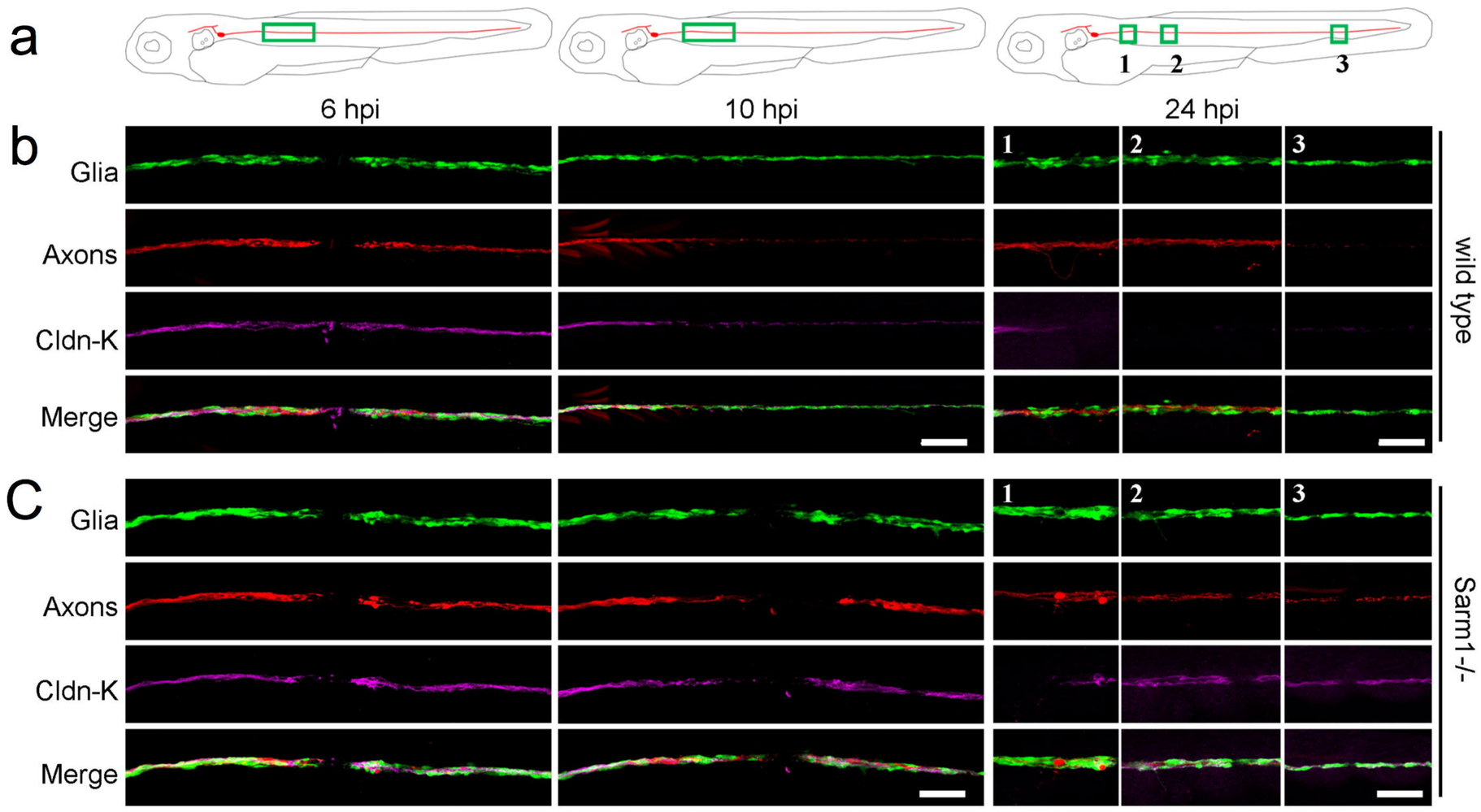
a
1
2
3
6 hpi
10 hpi
24 hpi
b
Glia
Axons
Cldn-K
Merge
wild type
C
Glia
Axons
Cldn-K
Merge
Sarm1-/-

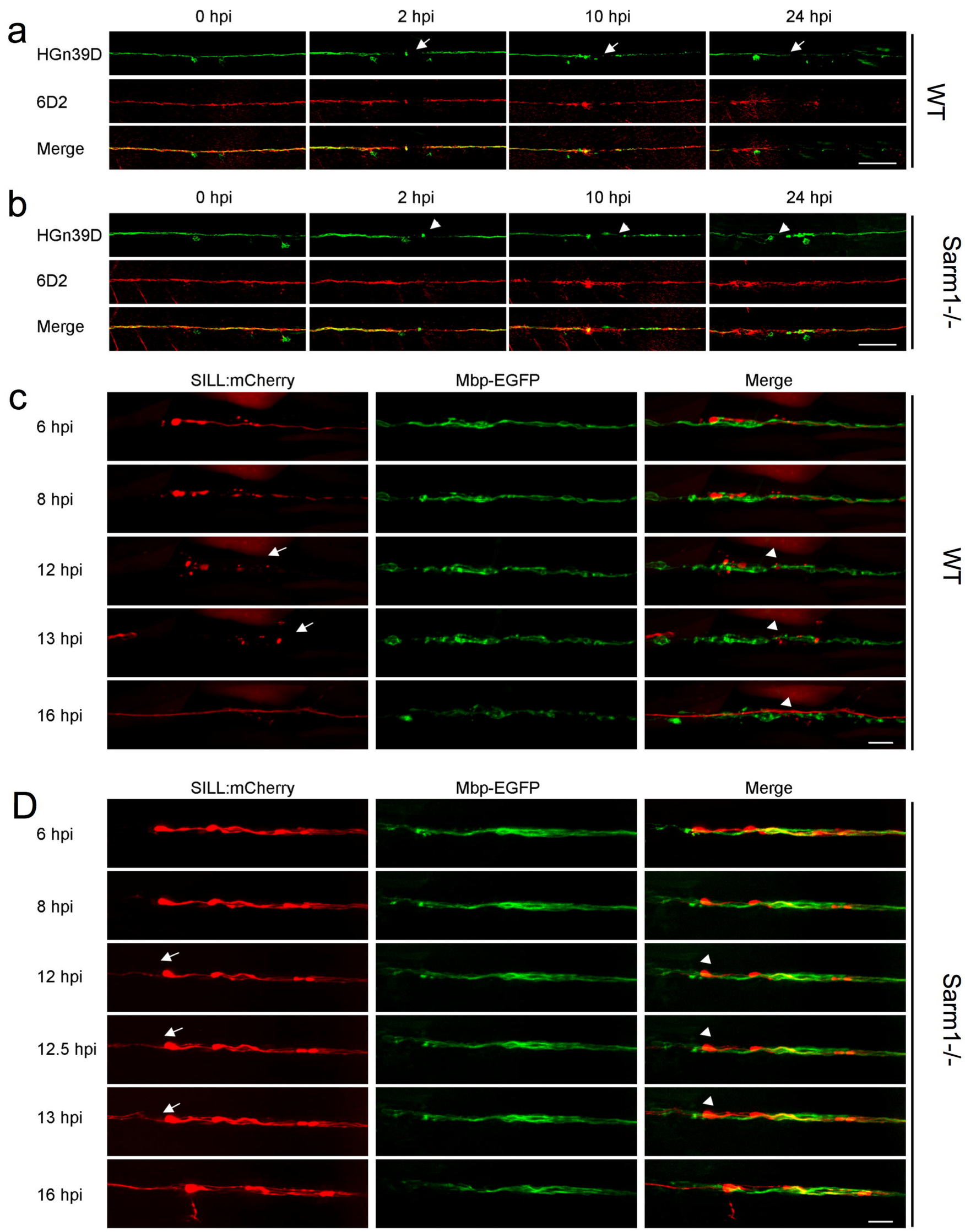
a
0 hpi
2 hpi
10 hpi
24 hpi
HGn39D
6D2
Merge
WT
b
0 hpi
2 hpi
10 hpi
24 hpi
HGn39D
6D2
Merge
Sarm1-/-
C
SILL:mCherry
Mbp-EGFP
Merge
6 hpi
8 hpi
12 hpi
13 hpi
16 hpi
WT
D
SILL:mCherry
Mbp-EGFP
Merge
6 hpi
8 hpi
12 hpi
12.5 hpi
13 hpi
16 hpi
Sarm1-/-

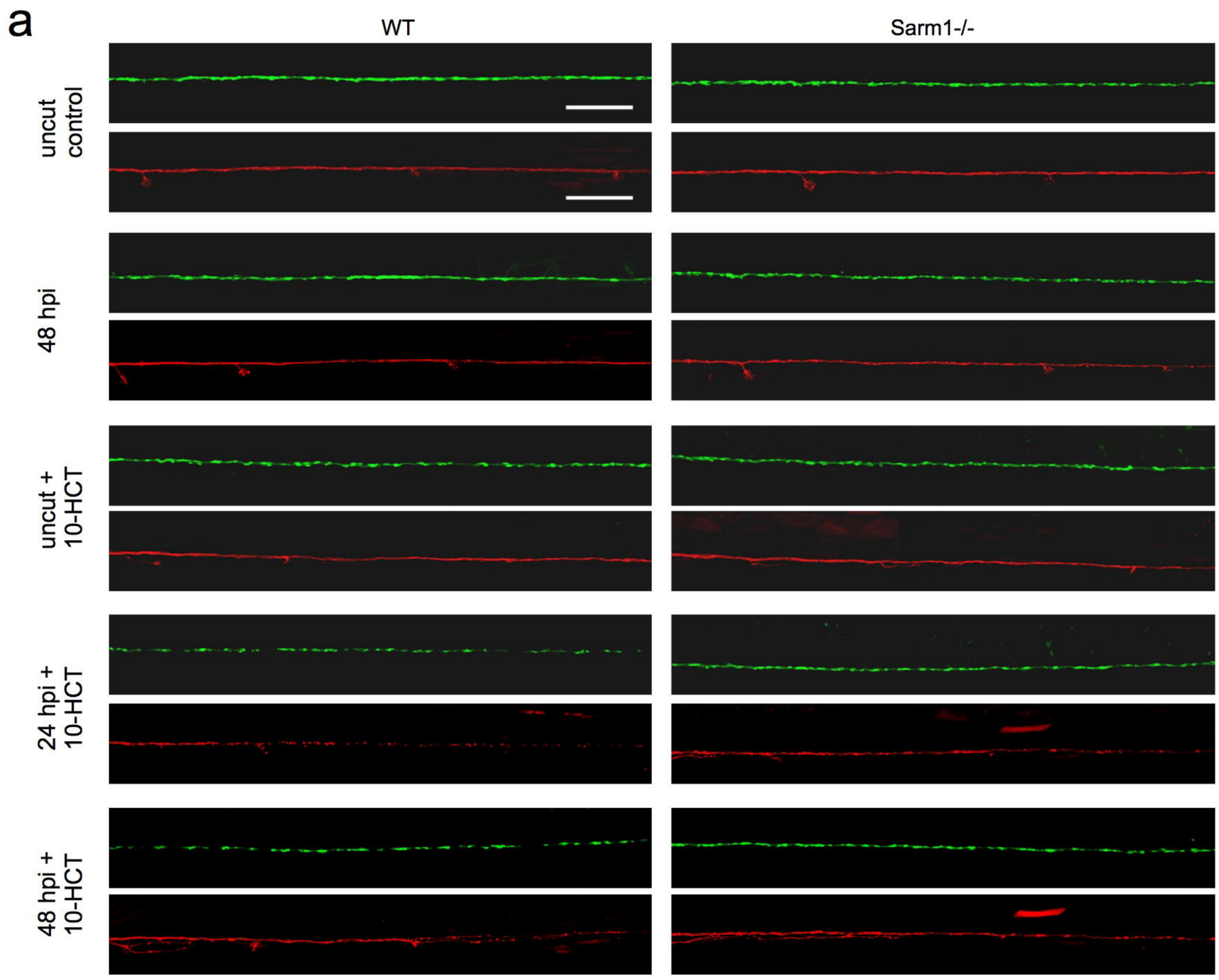
a
WT
Sarm1-/-
uncut control
48 hpi
uncut + 10-HCT
24 hpi + 10-HCT
48 hpi + 10-HCT

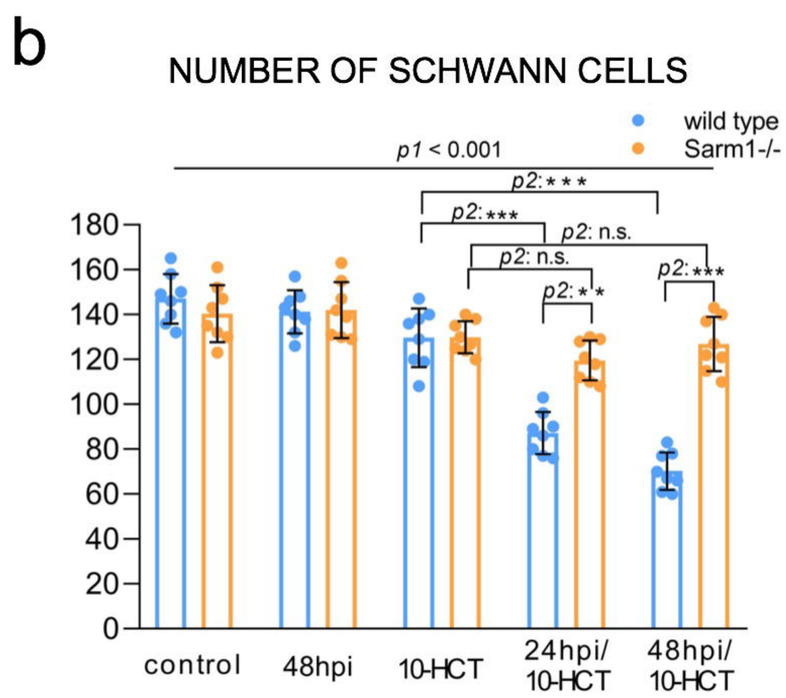
b
NUMBER OF SCHWANN CELLS
wild type
Sarm1-/-
p1 < 0.001
p2:***
p2:***
p2: n.s.
p2: n.s.
p2:**
p2:***
180
160
140
120
100
80
60
40
20
0
control
48hpi
10-HCT
24hpi/ 10-HCT
48hpi/ 10-HCT

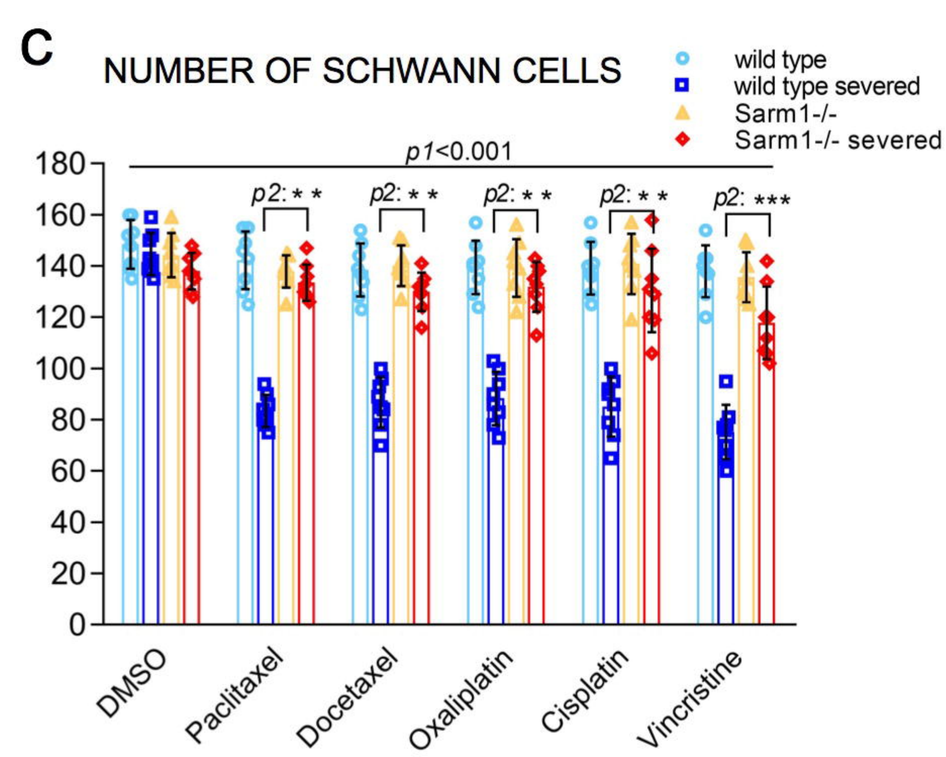
c
NUMBER OF SCHWANN CELLS
wild type
wild type severed
Sarm1-/-
Sarm1-/- severed
p1<0.001
p2:**
p2:**
p2:**
p2:**
p2:***
180
160
140
120
100
80
60
40
20
0
DMSO
Paclitaxel
Docetaxel
Oxaliplatin
Cisplatin
Vincristine

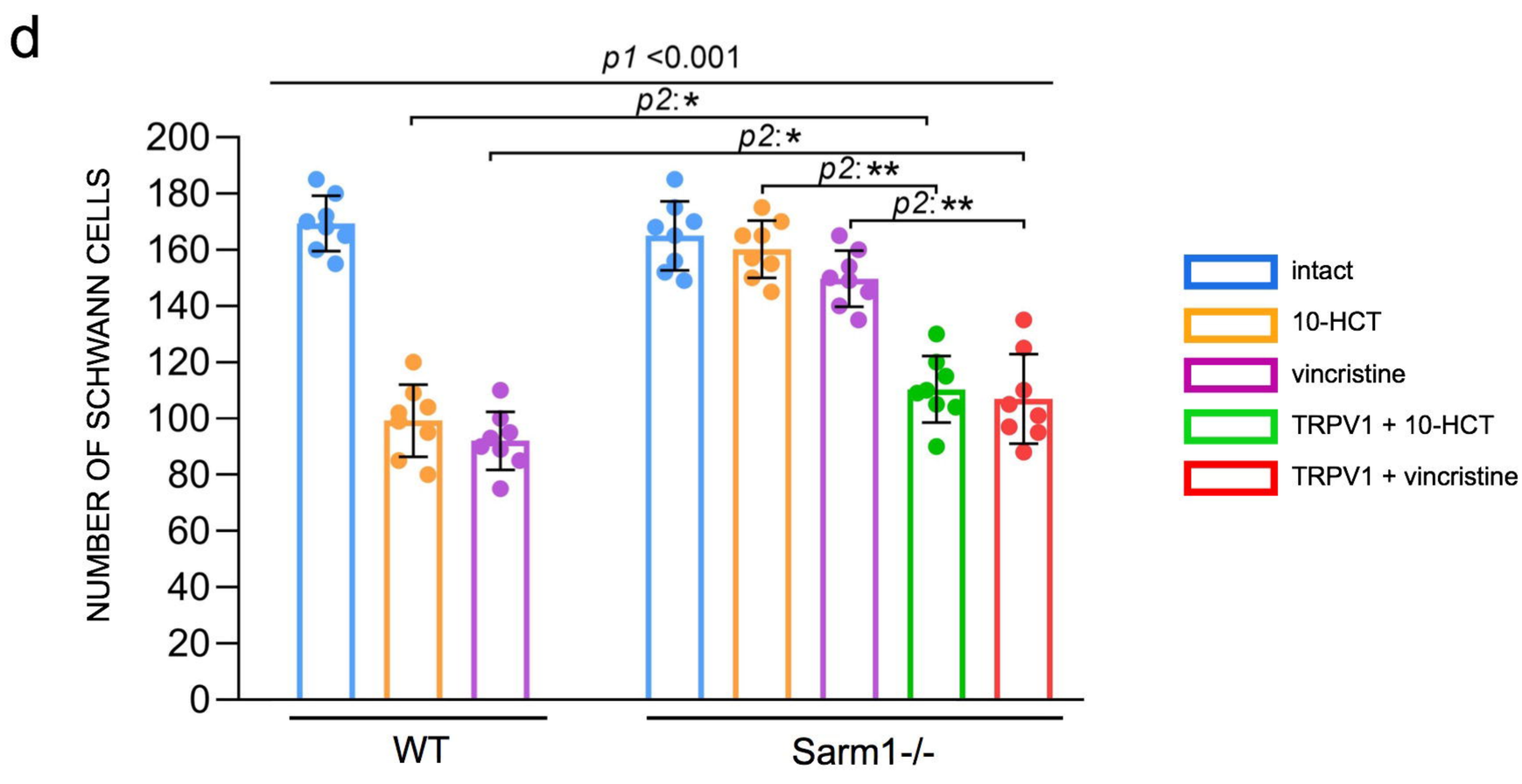
d
p1 <0.001
p2:*
p2:*
p2:**
p2:**
NUMBER OF SCHWANN CELLS
200
180
160
140
120
100
80
60
40
20
0
WT
Sarm1-/-
intact
10-HCT
vincristine
TRPV1 + 10-HCT
TRPV1 + vincristine